CONTINUOUS-WAVE COMB FOURIER TRANSFORM SPECTROSCOPY

by

Thilo Kraetschmer

A thesis submitted in partial fulfillment of the

requirements for the degree of

Master of Science

(Mechanical Engineering)

at the

UNIVERSITY OF WISCONSIN-MADISON

2006

ABSTRACT

Continuous-Wave Comb Fourier Transform Spectroscopy

Thilo Kraetschmer

Under the supervision of Assistant Professor Scott T. Sanders

at the University of Wisconsin-Madison

Due to its versatility, Fourier-transform spectroscopy (FTS) has found wide-spread application in research and development, monitoring of industrial processes, forensics, etc[1]; its uses continue to expand[2]. Despite decades of development and improvement of Fourier-transform (FT) spectrometers many of their attributes still show the potential for significant improvement. Two attributes that are of major significance for the performance of FT spectrometers are the increase of spectral radiance of the light sources employed in conventional spectrometers and the increase of measurement speed. Modern super-luminescent light sources offer superior levels of spectral radiance when compared to traditionally employed incandescent light sources. Due to this higher brightness, measurements with a higher signal-to-noise ration can be made. Also, the higher light throughput enables measurements at a higher repetition rate, so that the rate is ultimately limited by the dynamics of the (usually mechanical) scanning process employed in FT spectrometers. Repetition rates of up to 2 kHz can be achieved with rotating interferometers[3],

and non-mechanical interferometers exhibiting even higher repetition rates are under development[4].

An entirely different approach to high-throughput high-speed FTS was pursued by van der Weide et al.[5-7]. It is based on heterodyne frequency-comb spectroscopy and employs two frequency combs with slightly different mode spacing. This approach, termed frequency-comb Fourier-transform spectroscopy (c-FTS), relies on expensive mode-locked lasers but enables high-throughput FTS with demonstrated repetition rates of ~ 1 kHz. However, even in this case one has to rely on moving cavity mirrors[5].

This thesis presents a new approach to c-FTS that employs continuous-wave light sources (CW c-FTS). It combines the benefits of conventional FTS (broad spectral coverage, high throughput) with the following advantages: no moving parts, high repetition rate, and good signal-to-noise ratio (SNR) due to high spectral radiance sources. By engineering stable, broadband combs, CW c-FTS could result in a universal and simple approach for spectroscopy at almost arbitrary measurement speeds and spectral resolutions limited only by Fourier principles.

PREAMBLE

The bumble-bee's wing area is only 0.7 square centimeters but the bumble-bee has a mass of 1.2 grams.

Aerodynamically, the bumble-bee shouldn't be able to fly.

But the bumble-bee doesn't know that so it goes on flying anyway.

ACKNOWLEDGEMENTS

There are a lot of people I would like to thank for a huge variety of reasons.

First and foremost, I would like to thank Scott Sanders. I could not have imagined having a better advisor and mentor for my Master's studies here at the University of Wisconsin-Madison. Without his patient guidance, his intuition, perceptiveness and open-minded approach, I would never have been able to finish this work.

I would also like to thank Joachim Walewski, whose knowledge of heterodyning spectroscopy was essential for the development of CW c-FTS. He was the source of answers for my never-ending questions on spectroscopy and on the theory of Fourier transformations.

Thank-you to Laura Kranendonk, Renata Bartula, Drew Caswell, and Chris Hagen, for their advice with issues around the lab. This help was greatly appreciated; in particular, because I had absolutely no experience with optical equipment when I first started working in this research group.

Outside of the research group, I would like to thank my parents, family, and friends for their support and encouragement. Especially, I would like to thank my two grandmas for "pushing their thumbs" (German equivalent to "keep one's fingers crossed") for every single exam I took throughout my entire time in college. Without all that luck, I might have not ended up in graduate school, which is why it is to them that I dedicate this work.

This material is based on work supported by National Science Foundation grant CTS-0238633, Honda R&D, and by a Technology Innovation Fund from the University of Wisconsin-Madison Graduate School.

TABLE OF CONTENTS

TABLE OF FIGURES

LIST OF TABLES

CHAPTER 1. INTRODUCTION

1.1 OVERVIEW

The first chapter of this thesis is a stand-alone introduction to hyperspectral sensing and spectroscopy. Some applications of hyperspectral sensing are given that show the versatility of this sensing approach.

Chapter 2 addresses the question of how to measure a spectrum, shows different measurement techniques, and introduces the frequency downshifting idea, where a replica of the native spectrum in the optical frequency range is generated in the radio frequency range by heterodyning frequency combs.

The third and the fourth chapter present simulation and experimental results of two different CW c-FTS sources. Whereas the design presented in Chapter 3 allows CW c-FTS through the interference of two CW frequency combs, Chapter 4 focuses on beating of only one unequally spaced CW frequency comb.

Chapter 5 summarizes the work presented in this thesis and gives some suggestions for future research.

1.2 HYPERSPECTRAL SENSING

The term hyperspectral denotes a sensor system observing a target in different spectral bands. Two spectral bands is dual band, three to several is multispectral, more is hyperspectral (hyperspectral = “excessive; too many bands”[9]). Ultraspectral sensing[10] records even more bands than hyperspectral sensor systems (ultra = “beyond hyper”).

Hyperspectral sensing provides a continuous record of spectral responses of materials over the wavelengths considered. The spectral curve obtained from combining the different bands can then be matched with spectral signatures of individual materials from either field measurements or data bases to obtain information about the target. Among numerous fields of application, hyperspectral sensing is widely used in Earth surface measurements. Here, airborne hyperspectral sensor systems measure quantitatively the components of the Earth system acquired as images for scientific research. The general concept of imaging spectroscopy is depicted in Figure 1.1[9, 11].

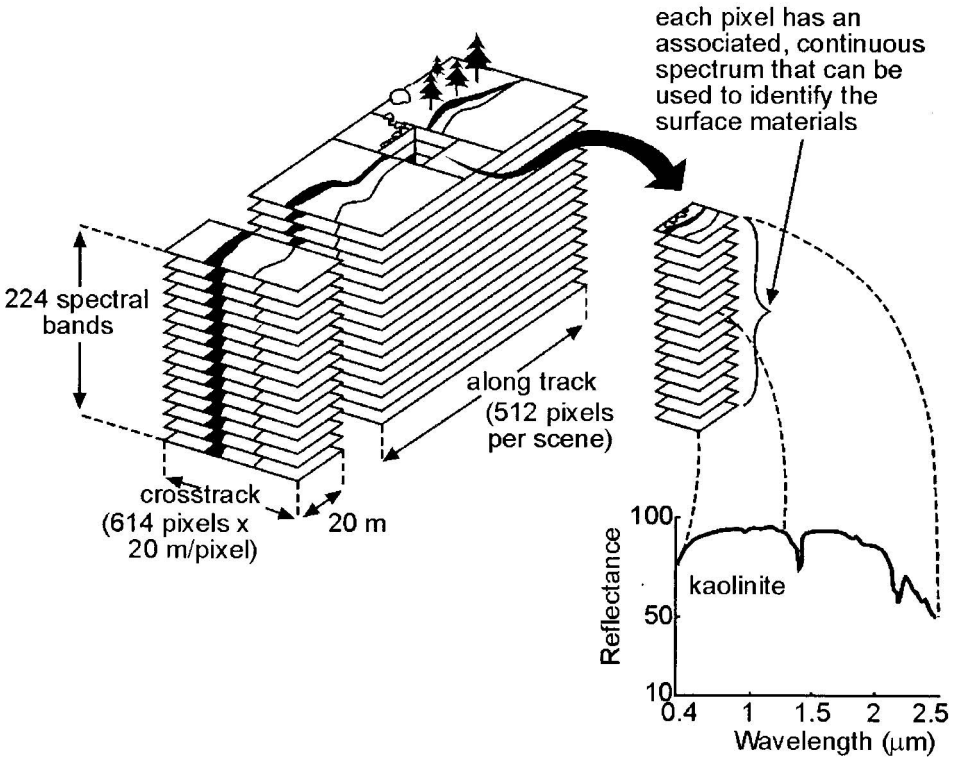

Figure 1.1 Concept of imaging spectroscopy as an example for hyperspectral sensing

Imaging spectroscopy acquires images in a large number where each corresponds to one band. For example, a slit is fixed in front of a 2-D camera so that only the first row of pixels

is ever illuminated. Then, the camera/slit assembly is translated above the stationary surface to be imaged. The first-row information is constantly stored and updated during translation. At the end of the translation, a 2-D grayscale image of the surface can be built from the stored information. To make this arrangement hyperspectral, the process is identical except that a diffraction grating is fixed between the slit and the camera so that columns contain spectral information. After translation, the image assembled from row 1 information contains a spectrally-filtered view of the surface; the image from row 2 contains a different spectrally filtered view, etc. This enables the extraction of reflectance spectra at a pixel scale.

Imaging spectrometry is used to identify a number of important rock forming minerals[12], and for geologic mapping and studies of volcanoes[13]. More examples include the monitoring of oil spills, pulp mill effluent or schools of fish in coastal zone oceanic regions as well as studies of vegetation[14].

The theory that correlates the spectrum of a material with its physical attributes is spectroscopy.

1.3 SPECTROSCOPY

Spectroscopy may be defined as the study of the interaction of electromagnetic waves and matter[15]. It is the study of spectra, that is, the dependence on physical quantities on frequency, or rather color. Spectroscopy is used for the identification of substances and their physical attributes, through the spectrum emitted or absorbed. The article of interest is matter that is made up of atoms and molecules. Atoms are composed of nuclei containing protons, neutrons, and electrons surrounding the nuclei. Hence matter includes a large quantity of oscillators of very different dimensions. Like mechanical or electrical oscillators, these can

be excited to a higher level using the appropriate energy and frequency. So when light interacts with matter, light of certain wavelengths is absorbed while at other wavelengths is transmitted in the substance[2]. One way to classify spectroscopy is by the measurement process. The four most common generic spectroscopy arrangements are depicted in Figure 1.2.

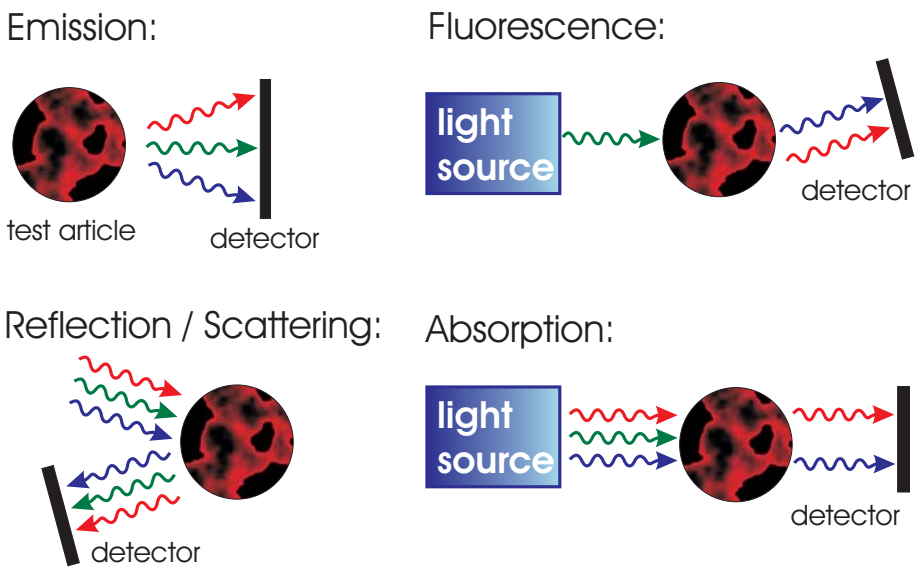

Figure 1.2 Four most common generic spectroscopy arrangements: Emission, Reflection / Scattering, Fluorescence, and Absorption.

- **Emission Spectroscopy** is the study of electromagnetic spectra in which a test article radiates. Atoms or molecules give off radiation as they undergo a transition from a higher energy level to a lower energy level. The energy that is needed to achieve the excitation level can be from a variety of sources such as chemical reactions or collision. The main drawback of emission spectroscopy is the low radiation intensity, in particular when examined at high resolution. The lower the temperature of the test article, the lower the intensity of radiation. Therefore, this non-intrusive sensing

approach is used for sensing of hot test articles e.g. the constant monitoring of plasma conditions during fabrication processes[16].

- **Fluorescence Spectroscopy:** In fluorescence spectroscopy, the test article is being excited by absorbing higher energy photons which causes emitting of lower energy photons. The physical quantities obtained from the detected spectrum are in general more of a qualitative nature. Another drawback of this spectroscopic measurement is that dependent on the test article, fluorescence-stimulating seed has to be added to the system which may alter the performance of the system. Fluorescence spectroscopy has found wide-spread application in sensing e.g. biochemical and medical processes[17].

- **Absorption Spectroscopy:** In order to get information about the test particle through absorption spectroscopy, the test article has to be partially transparent to radiation. Because different molecules have different frequencies where absorbance takes place, measuring the absorption spectrum yields information about the molecular composition and hence, physical quantities of the material can be derived.

- **Reflection / Scattering Spectroscopy:** If the test article does not radiate by itself and if it is not transparent to radiation, reflection or scattering spectroscopy can be used to obtain a spectrum. As the incoming radiation is merely reflected, it has to reach the surface of the test article and be reflected from it. Hence, the radiation must pass twice through any molecules adsorbed on the surface. The resulting path length, although it is extremely small, is still sufficient to get an absorption spectrum of the test article[15]. Among a wide field of applications, reflection / scattering spectroscopy

is used for planet surface imaging. The NASA Infrared Telescope Facility (IRTF) obtained infrared imaging spectroscopy data of Mars in June, 2003, using the Texas Echelon Cross Echelle Spectrograph (TEXES). A map of surface temperature and of H_2O could be retrieved[18].

All four types of spectroscopy mentioned above are measuring the spectrum of a test article. However, the 'emission' case is considered passive while the remainders are considered active because they use external light sources. Engineering of a hyperspectral light source that can be used for spectroscopic measurements is the topic of this work.

1.4 MOTIVATION FOR ENGINEERING A HYPERSPECTRAL LIGHT SOURCE

The motivation question has to be asked since most absorption spectroscopic measurements can be made using only a light bulb as a thermal emitter, a test article, and a spectrometer to measure the spectrum. However, using a hyperspectral light source for spectroscopic measurement entails some major advantages:

- **Efficient at high resolution:** Whereas there is a trade-off between spectral resolution and collection etendue in the "light bulb & spectrometer" setup, for a hyperspectral light source, these two attributes are decoupled. For the latter case, the linewidth of the source determines the spectral resolution independently from the detector. As a result of that, beamsteering does not compromise spectral resolution.

- **Simple, rugged, compact, all-fiber:** Hyperspectral light sources are more readily multiplexed than hyperspectral detectors, e.g. for multi-beam tomography.

- **Compatible with simple detectors, thus not paced by camera technology:** For spectroscopic measurements, cameras still show limited readout rates, and furthermore, they are usually optimized for the visible range.

- **Can complement spectrometers:** Hyperspectral light sources can be combined with spectrometers, e.g. for combined excitation-emission fluorescence spectroscopy.

- **Ordered light eliminates natural beating:** The interference of light emitted by incoherent emitters causes noise because the low frequency part of natural beating lies within the bandwidth of the detector. This beating is eliminated for ordered light emitted by appropriate lasers.

CHAPTER 2. COMB FOURIER TRANSFORM SPECTROSCOPY C-FTS

This chapter deals with the measurement of spectra. It addresses the question of how to measure a spectrum, shows different approaches, and introduces the heterodyning idea.

A hyperspectral light source that gives the opportunity to measure a spectrum can be characterized by the following three main criteria:

- **Spectral coverage:** The spectral range of the hyperspectral light source. A broad spectral coverage is necessary to detect multiple species with a single source. Also, a broad coverage allows monitoring of broad spectral features (heavy or high-pressure gases, supercritical fluids, liquids, solids, etc.).

- **Resolving power:** The spectral resolution of the hyperspectral source is the ability to resolve features in the spectrum. It can be defined by $R = \frac{\Delta\lambda}{\lambda}$ where $\Delta\lambda$ is the smallest difference in wavelengths that can be distinguished at a wavelength λ. The discrimination of multiple species highly depends on resolving power. In optical coherence tomography (OCT) a higher resolving power enables a larger ranging depth: 1 cm^{-1} resolution enables 3.7 mm-deep images, 20 cm^{-1} resolution only allows 185 μm-deep images.

- **Repetition rate:** The time it takes to make one measurement of a spectrum. A high measurement speed, and thus a high information rate, provides immunity to low-frequency noise sources, e.g. vibrations, beamsteering, etc. High repetition rates are

necessary to monitor transient systems (explosions, shock tubes, pulsed magnetic fields, video-rate OCT, etc.)

Needless to say, there is a trade-off between these three criteria. For example, it is easier to achieve high resolution over a narrow spectral range than over a broad wavelength range. In the following, a whish list for a new source will be created by having a closer look at already existing hyperspectral light sources.

2.1 EXISTING SPECTROMETERS NOT BASED ON C-FTS

In this section, two different hyperspectral light sources will be shown. The first one has been recently developed and provides spectral encoding in time, that is to say, the bands are recorded successively in time. By contrast, the second example measures all bands at the same time, retrieving the information of each band via a Fourier transformation. Hence, this measurement technique provides spectral encoding in frequency.

2.1.1 Fourier domain mode locked amplifier (spectral encoding in time)

Fourier domain mode locking (FDML) was recently presented by Huber et al.[19] as a new technique for frequency-swept laser operation. FDML is comparable to active laser mode locking for short pulse generation, except that the spectrum rather than the amplitude of the light field is modulated. A FDML laser is constructed using a long fiber ring cavity, a semi-conductor optical amplifier, and a tunable fiber Fabry-Perot filter as depicted in

Figure 2.1. The optical band-pass filter is driven synchronously with the optical round-trip time of the propagating light wave in the cavity. By so doing, light from one frequency sweep travels through the cavity and returns to the band-pass filter when the transmission of

the filter is at the same spectral position. At the optical band-pass, the electric field has only frequency components that match the transient filter transmission, while all other frequency components destructively interfere. This produces a quasi-stationary lasing operation. Taking a spectral snapshot of the cavity would show that all colors in the wavelength range of operation are present at all times but circulating at different positions with the same speed.

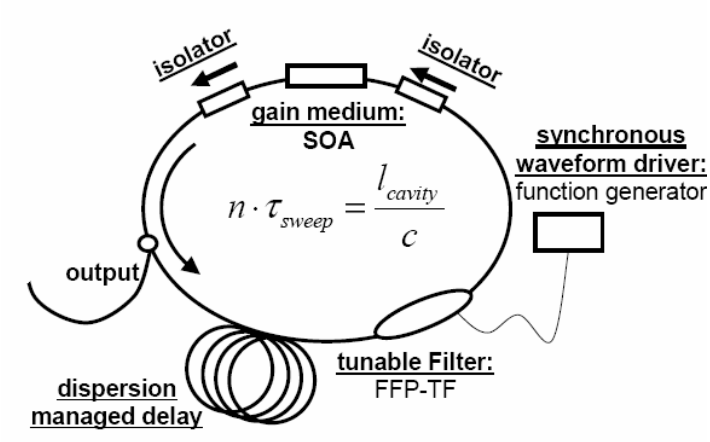

Figure 2.1 Schematic of the Fourier domain mode locked frequency-swept laser. The cavity consists of a semi-conductor optical amplifier (SOA), two isolators, a dispersion managed delay to achieve a low dispersion across the wavelength range of operation, and a tunable Fabry-Perot Filter (FFP-TF)..

High-speed, narrowband optical frequency sweeps are generated with a repetition period equal to the fundamental or a harmonic of the cavity roundtrip time. Sweep rates of up to 290 kHz were demonstrated with a 105 nm tuning range at 1300 nm center wavelength (see Figure 2.2).

One application of this frequency-swept laser is swept-source optical coherence tomography (OCT) imaging. A 3-D OCT data set of a human finger *in vivo* is shown in Figure 2.3. The FDML laser was operated at a modulation frequency of 116 kHz. The physical cavity length was 7 km, which corresponds to a fundamental roundtrip frequency of 29 kHz. The

256x128x256 pixel volume was recorded at 232,000 axial scans/s, 906 frames/s, and 3.5 volumes/s.

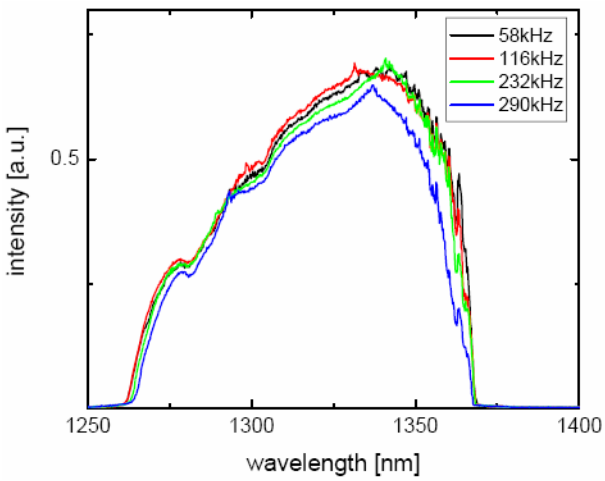

Figure 2.2 Integrated spectra of the FDML source for different effective sweep rates. Note that the spectral shape of the transient intensity profile does not change much as the driver frequency is increased.

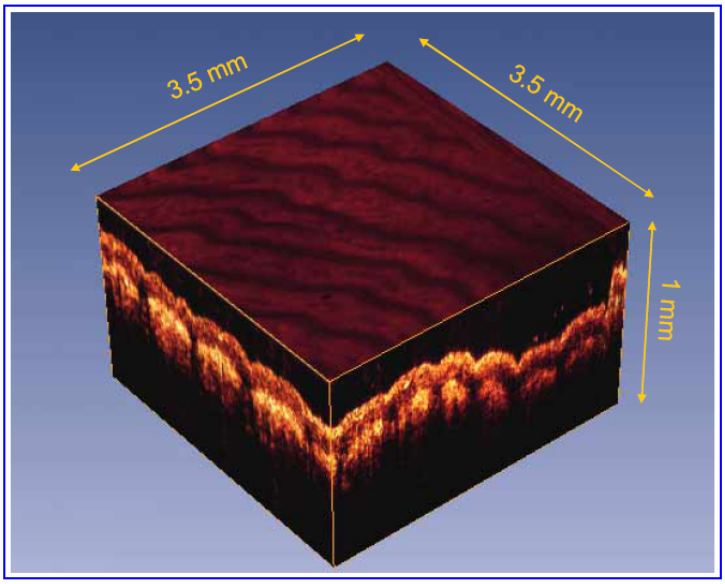

Figure 2.3 Human finger *in vivo*. 3-D data set acquired in 0.28 s. The 256x128x256 pixel volume was recorded at 232,000 axial scans / s, 906 frames / s, and 3.5 volumes / s. The picture shows a volume-rendered representation of the 3-D OCT data set (1.4MB).

The main advantages of this hyperspectral light source are: high repetition rate, rather inexpensive setup (<$25k), and the consistent dependency of wavelength and time. However, in addition to undesirable polarization effects, the setup includes moving parts (FFP-TF). Also, the sweep rates are constrained to the fundamental and harmonics of the cavity resonance frequency and limited by the piezo actuator (peak ~ 300 kHz). Furthermore, the lasing operation can only take place inside of telecom bands, because the setup requires fiber with near-zero dispersion, which is difficult to achieve outside the telecom range.

2.1.2 Fourier transform spectroscopy (spectral encoding in frequency)

Compared to the recently developed hyperspectral light source presented above, Fourier transform spectroscopy (FTS) already has a long history. The development of FTS would have been impossible without the Michelson interferometer, which was invented in 1880 by Albert Abraham Michelson[20]. He won the Nobel Prize in Physics for accurately measuring wavelengths of light using his interferometer. The drawback to interferometric instruments is that they do not give the spectrum directly but its Fourier transform. An inverse Fourier transformation is required to derive the desired spectrum. In Michelson's era, the calculations used to convert an interferogram into a spectrum were very time consuming. That changed with the invention of computers in combination with the "Fast Fourier Transform" (FFT), an algorithm first discovered by Gauss in 1805[21] and then rediscovered by J.W. Cooley and J.W. Tukey in 1965[22].

The basic principle of an interferometer is to take a beam of light, split it in two beams, and make one of them travel a different distance than the other [23]. An optical diagram of a

Michelson interferometer that, in some form, is still present in most Fourier transform spectrometers is presented in Figure 2.4.

Broadband light coming from a source hits the beam splitter *BS* and is divided in two parts. The part that is reflected strikes a fixed mirror *M1,* whereas the part that is transmitted strikes a moving mirror *M2*. The difference in distance traveled by these two beams is called optical path difference δ. The two parts are recombined at the beam splitter, interfere with each other and interact with the sample before they strike the detector.

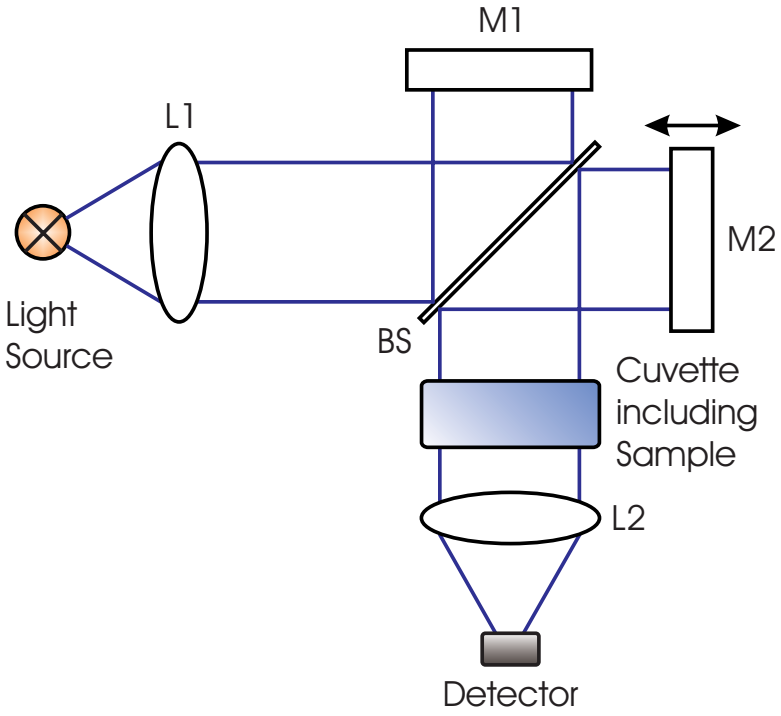

Figure 2.4 Schematic of a Michelson interferometer including a light source, two lenses (L1, L2), a cuvette, a beam splitter (BS), one fixed mirror (M1), one moving mirror (M2), and a detector.

Assuming a monochromatic light source of wavelength λ and a constant mirror *M2* velocity, the intensity vs. δ profile is a cosine waveform with a period of λ because of constructive and destructive interference at the beam splitter. The beam is modulated in the interferometer

with the modulation frequency $f_{\mathrm{mod}} = 2v_{M2} / \lambda$, where v_{M2} is the moving mirror velocity and λ is the wavelength of the light beam. Hence, every color emitted by the broadband light source is modulated at a unique frequency.

A simplistic way to think about the process is that the interferometer encodes the intensity and wavelength information so all the data can be measured at once, and a Fourier transform decodes the information to obtain the spectrum.

2.1.3 Comparison of time vs. frequency based techniques

There are a number of advantages to be gained by using "spectral encoding in frequency"-rather than "spectral encoding in time" measurements[15]. Please note here that some of the following general points may not apply to specific hyperspectral light sources.

- **The multiplex or Fellgett advantage**[24]. For spectral encoding in time measurements, each resolution element is scanned consecutively, so for a total scan time *T*, the time *t* that it takes to record one resolution element is *T* / *n* where *n* is the number of resolution elements. For spectral encoding in frequency measurements, the entire spectrum is recorded for the whole total scan time *T*. Only considering noise from the data acquisition (DAQ) system, SNR is proportional to the square root of the measurement time. Thus, the multiplex advantage gives a gain of $\sqrt{n}$ in signal-to-noise for spectral encoding in frequency if the light source is stable and noise is only contributed by the DAQ system. However, as spectral encoding in frequency has a multiplex advantage in signal, it also has a multiplex disadvantage in noise, if the

noise is induced by the light source. A stable light source is essential for spectral encoding in frequency measurements.

- **The throughput or Jacquinot advantage**[25]. In a dispersive instrument the radiation is brought to a focus on a slit. A very fine slit gives good resolving power since only a narrow spread of frequencies are recorded at any moment. A side effect of this is that the total amount of energy in the instrument is limited, requiring 'noisy' amplifiers. In FT measurements all the source energy passes through the instrument and thus, amplifiers are less critical.

- **Resolving power**. In a grating or prism instrument, the resolving power depends on the angle at which the radiation beam strikes that component, and hence varies with frequency. The resolving power for an FT instrument is constant over the whole spectrum.

The three main drawbacks of FTS instruments that include any related form of a Michelson interferometer are:

- **Moving parts**. In order to guarantee a correct encoding of the spectrum, the control of the moving parts has to be very precise. Moving parts ultimately limit the repetition rate of the measurement; also, typical long dwell times between subsequent interferograms further reduces the measurement speed.

- **Weak light sources**. In general, weak and incoherent blackbody sources are employed in conventional spectrometers. This limits the attainable focus size in infrared microscopy, and also the stand-off distance in remote sensing applications[5].

- **Low measurement speeds**. Although the repetition rates of FTS were significantly improved in recent developments (repetition rates up to 2 kHz were achieved with rotating interferometers[3]) the measurement speed is ultimately limited by the scanning speed of the mirror.

2.1.4 Wish list for a new laser design

For a design of a new hyperspectral laser, it is desirable to combine the advantages of the two different approaches given in the section above and discard the drawbacks. This yields a wish list for a new hyperspectral light source:

- **Spectral encoding in frequency.** This approach seems to be very desirable, mostly because of the overall more universal nature and the multiplex advantage that, assuming a stable light source, improves SNR, which has a high impact factor on the performance of high speed measurement systems.

- **Broad, high spectral resolution light source.** A light source with these features is necessary to achieve high throughput, good SNR, and broad spectral coverage. Furthermore, a light source with a broad spectral coverage and a high spectral resolution allows detection and discrimination of multiple species and monitoring of broad spectral features.

- **High repetition rate.** High measurement speeds offer immunity to “slow” noise sources and enable measurements in dynamic environments, e.g. gas dynamics (engines, shock tubes, explosions, turbo-machinery, pulse tubes, etc.), chemical kinetics or high-Tesla magnetic fields studies. Also, the high repetition rate of the

hyperspectral light source makes it suitable for scanning experiments in relatively steady environments, i.e. for the acquisition of multi-scalar images.

- **No moving parts.** Moving parts are degrading the overall performance of a hyperspectral light source in many ways: Motion control and dwell times issues, limiting of the repetition rate, etc.

Because the Michelson interferometer encodes the spectrum but involves moving parts, a new modulation method of a spectrum is needed.

2.2 HOW TO MODULATE A SPECTRUM

Measuring all bands at the same time, results in a time domain signal that basically looks like noise. Hence, the information of the spectrum, whose native frequencies reside in the THz-PHz range, has to be encoded such that the spectral information can be retrieved through post processing of the captured data. By using a detector with an infinite bandwidth, a pure FFT of the time domain signal would suffice. However, the bandwidth needs are by far not met by any detector available today. Thus the spectral information of each band has to be assigned to a lower frequency that lies within the bandwidth of a commercially available detector.

Some of the possibilities of how to modulate a spectrum are presented below.

2.2.1 Interferometer

As shown in 2.1.2, an interferometer encodes the spectrum through the constructive and destructive interference of light beams that have an optical path difference. The path difference is generated by the combination of a fixed and a moving mirror. However, this modulation approach relies on moving parts.

2.2.2 Rotating modulating collimator

A rotating modulating collimator (RMC) uses rotating shadow masks to modulate the count rate of photons from the source. The RMC technique was developed by Mertz[26] and found application in x-ray imaging[27]. A coaxial pair of grid-shaped masks modulates the incoming spectrum as a function of the radius r and the azimuth angle ϕ about the rotational axis (see Figure 2.5).

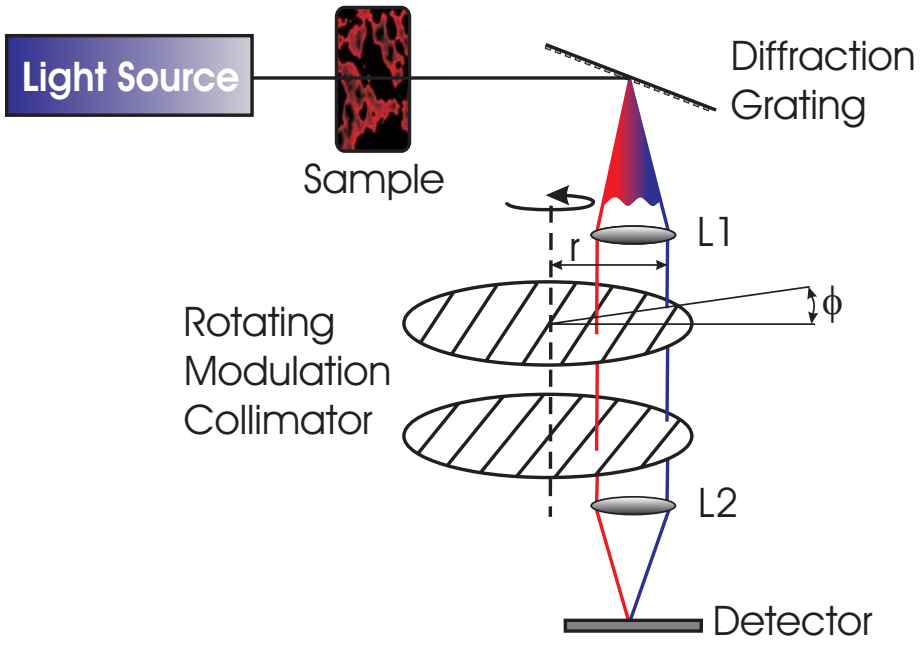

Figure 2.5 Simplified schematic of rotating modulation collimator in an absorption spectroscopy setup. The intensity of the incoming spectrum is modulated as a function of the radius *r* and the azimuth angle ϕ about the rotational axis. The frequency of the modulation is set by *r*, while ϕ sets the phase.

Assuming a single incoming beam to the RMC, Figure 2.6 shows how the resulting modulation profiles depend on source intensity, location and size[28]. The first panel shows the modulation profile of a single point source. The second panel shows the linear relation between input and output intensity. The azimuth angle ϕ is directly correlated with the phase

of the modulation, (panel 3), whereas a bigger distance from the rotational axis results in a higher modulation frequency (panel 4). Increasing the diameter of the source while keeping its intensity constant, reduces the amplitude of the modulation (panel 5 and 6). The modulation of a more complex source is shown in the last panel.

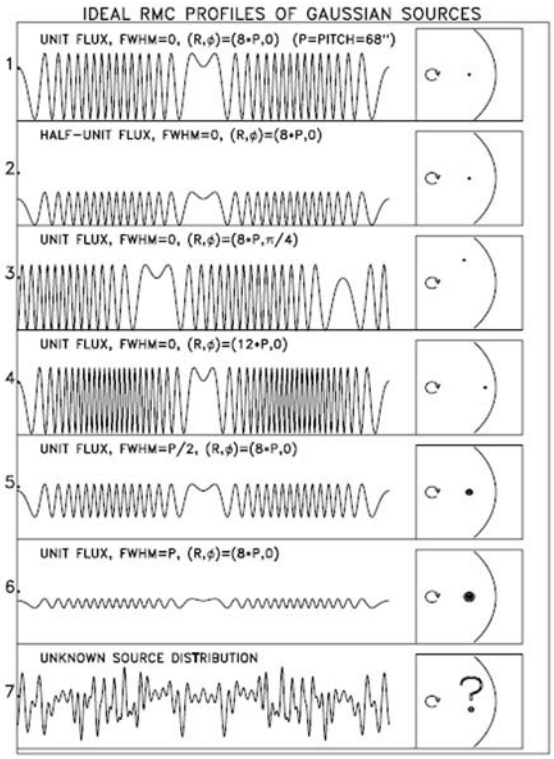

Figure 2.6 Modulation profiles simulated for one complete rotation for various configurations of an off-axis source, assuming ideal grids with equal slits mounted on a collimator that is rotating uniformly about a fixed axis.

Because of the angular dispersion of the diffraction grating, each band has a unique distance to the rotational axis and thus its own modulation frequency. Hence, the information can be decoded using FFT algorithms.

However, this approach includes moving parts and therefore doesn't meet the demands for the hyperspectral light source stated in the wish list above.

2.2.3 Diode laser array

The intensity of a monochromatic diode laser can be modulated with current. Using multiple monochromatic lasers, each current modulated at a different frequency, yields a hyperspectral light source. The setup of such a diode laser array as it could be used for absorption spectroscopy is depicted in Figure 2.7.

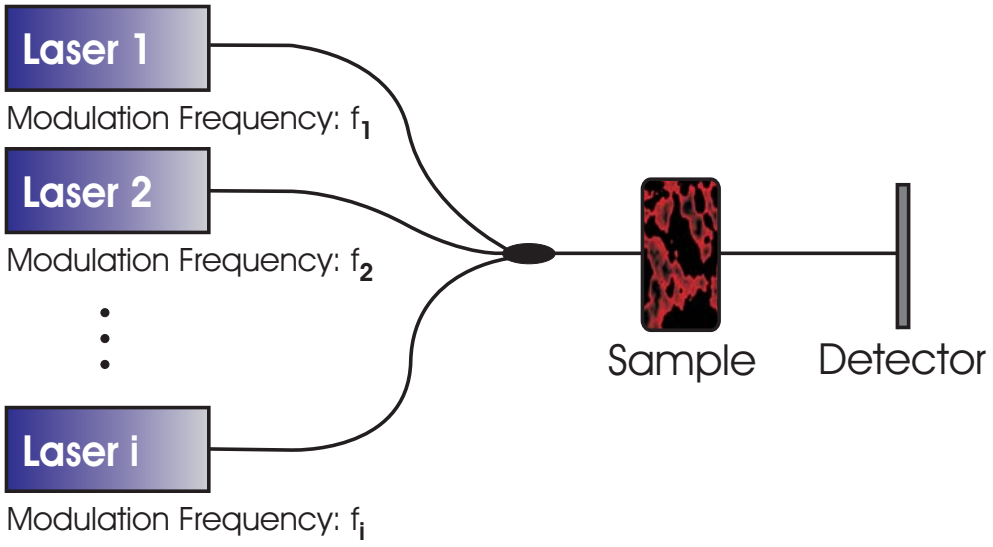

Figure 2.7 Setup of a laser diode array. The current of each monochromatic laser (1, …, i) is modulated at a different frequency, so that the information for all bands can be decoded with FFT algorithms.

This modulation technique does not involve any moving parts; however, the number of bands corresponds to the number of diode lasers and frequency generators, which makes this approach infeasible.

2.2.4 Optical beating with frequency combs

Mixing two or more signals generates new frequencies, which is referred to as heterodyning. The interference of each two frequencies results in the creation of two new frequencies, one at the sum of the two frequencies mixed, and the other at their difference. A low frequency produced in this manner is referred to as a beat frequency. This phenomena was first discovered in acoustics in 1740 by the Hamburg organist Georg Andreas Sorge and independently soon after by Guiseppe Tartini who described the beating tone with "il Terzo Suono" (the third sound). The effect was first observed with light in 1955 by Forrester, Gudmundsen, and Johnson[29].

An example for beating is given in Figure 2.8., where two electrical fields with the same amplitude but slightly different frequencies f_1 and f_2 interfere.

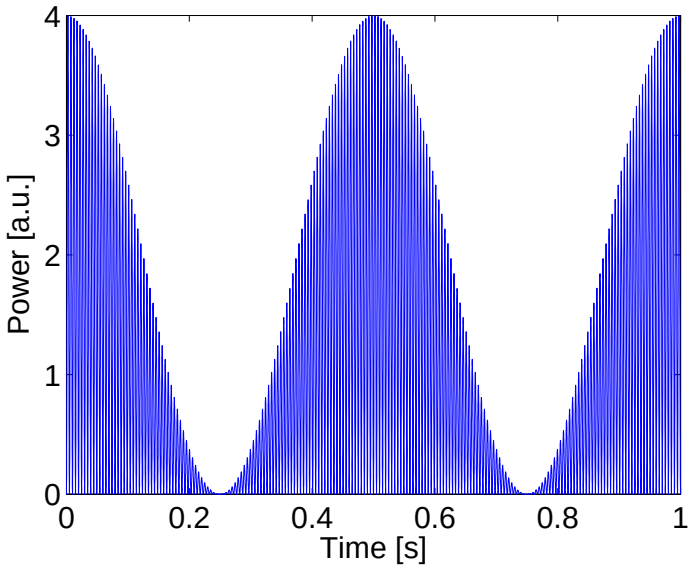

Figure 2.8 Intensity profile of two electrical fields E_1 and E_2 with constant amplitudes $A_1 = A_2 = 1$ and frequencies $f_1 = 100$ Hz and $f_2 = 102$ Hz. The beating signal with a frequency of 2 Hz as well as an additional DC component can be clearly seen.

A beating signal can be observed with a frequency equal to $\Delta f = f_1 - f_2$ and an additional DC component. A more thorough analysis of beating will be presented in the next section.

To ensure the feasibility of optical beating, a basic beating experiment was set up that shows beating of two almost monochromatic diode lasers (Lucent laser module, E2505D21). The interference of the two lasers was monitored with an optical spectrum analyzer (OSA) and an oscilloscope (OSC) as depicted in Figure 2.9. The temperature of both laser modules was controlled in a way that the two modules were lasing over the same wavelength range. Then the current of one laser was modulated with a triangular waveform (f_{mod} = 100 Hz) to achieve an oscillation of the lasing spectrum around the other one that was held constant.

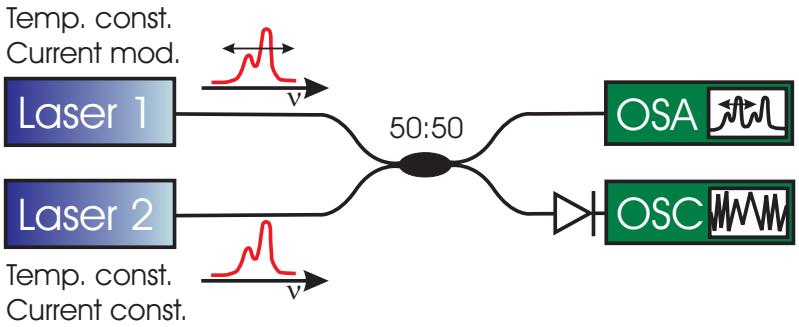

Figure 2.9 Setup for a basic optical beating experiment. Temperature control was used to achieve coverage of the two lasing spectra. To get a beating signal with a frequency that is dependent on time, current of laser 1 was modulated with a triangular waveform such that the lasing spectrum of laser 1 oscillated around the lasing spectrum of laser 2. The experiment was monitored with an optical spectrum analyzer (OSA) and an oscilloscope (OSC).

The results of this basic beating experiment can be seen in Figure 2.10. The lasing spectra of both laser modules captured with an OSA can be seen in Figure 2.10(a). This data was taken when the two spectra were the furthest apart. At this configuration, the amplitude of the interference signal at the oscilloscope is at its minimum because the native frequencies and

the beating frequencies are above the bandwidth of the data acquisition system (OSC: Tektronix TDS7404; 4 GHz bandwidth, 20 GSample / s; New Focus 1592; 3.5 GHz bandwidth).

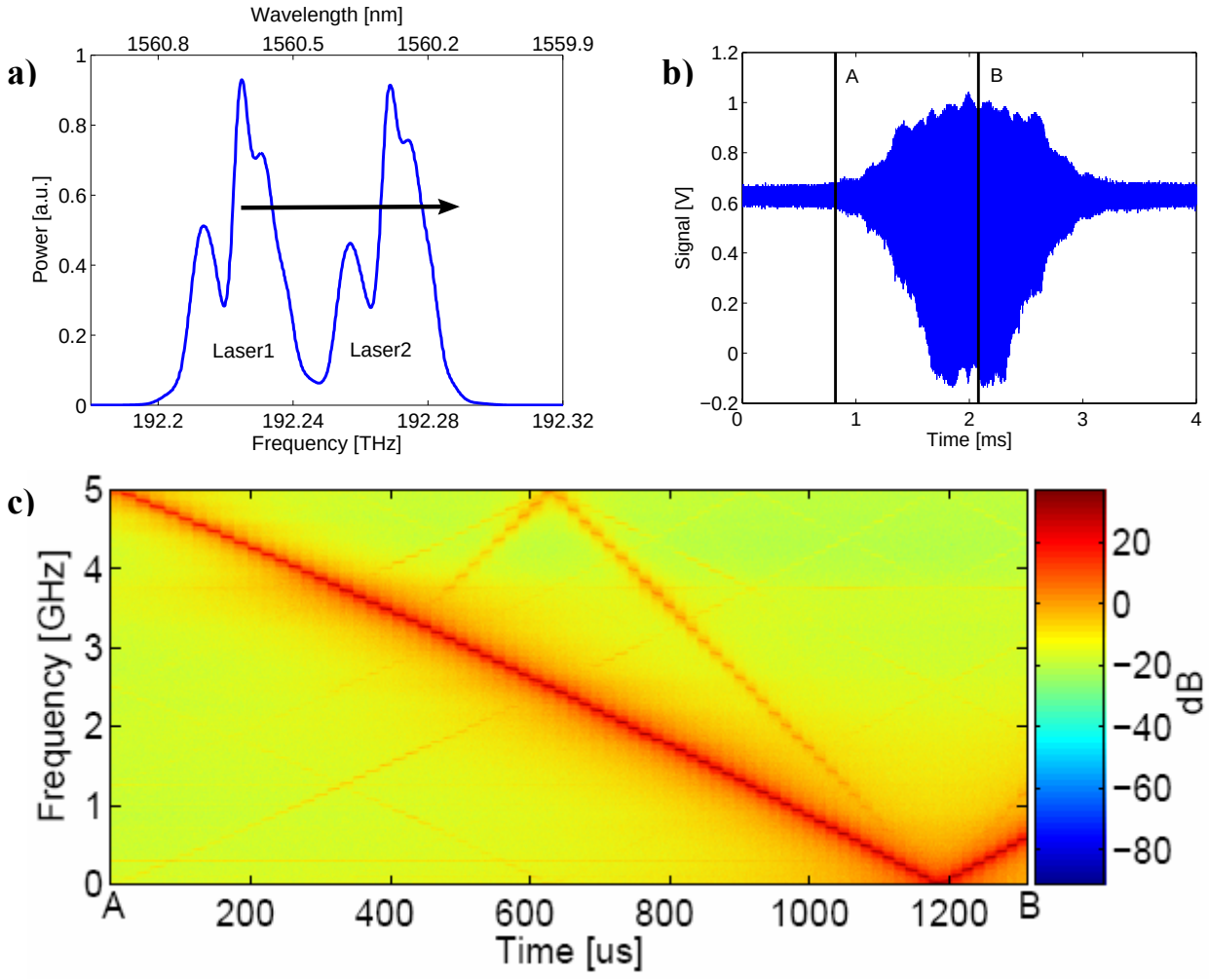

Figure 2.10 a) Lasing spectra of laser 1 and laser 2 recorded with an OSA. b) Time trace of the beating signal with complete coverage of the two lasing spectra shortly before *B*. c) Time-frequency plot of time trace *A*-*B*. The closer the two lasing spectra are, the lower the frequency of the beating signal. The minimum frequency is reached when the two lasing spectra are on top of each other.

The data on the oscilloscope was captured with a sampling rate of 100 ps per point, which corresponds to a Nyquist frequency of 5 GHz. As the two lasing spectra are getting closer,

the frequency of the beating signal decreases and passes the Nyquist frequency at *A* (see Figure 2.10(b)). The two spectra are on top of each other shortly before *B*. The time-frequency plot of the time trace *A–B* is shown in Figure 2.10(c). The beating signal can be clearly seen as well as its first harmonic and some aliasing artifacts.

In order to encode a spectrum by beating, the continuous spectrum has to be discretized in a way, such that frequency pairs emerge in the native optical spectrum. Beating of one of these pairs will produce a signal with an amplitude equal to the geometrical mean of the two amplitudes but at a lower frequency that can be measured with a photo receiver. Hence, each beating pair corresponds to a single band of the spectrum. Generating multiple beating pairs, where every pair beats at a unique frequency, results in a hyperspectral light source.

A frequency comb, which may be defined as an optical spectrum consisting of equidistant lines, gives a discretized version of an optical spectrum. Frequency combs is a hot topic in research, in particular, after the Nobel Prize in physics was awarded to Roy J. Glauber, John L. Hall, and Theodor W. Haensch in 2005. However, each pair of adjacent lines, or rather fringes, beats at the same frequency because of the equidistant fringes of a frequency comb. A light source has to be designed that generates interfering pairs with unique beating frequencies. The next sections shows one realization that employs two mode locked lasers.

2.3 MODE-LOCKED COMB FOURIER TRANSFORM SPECTROSCOPY C-FTS

A new hyperspectral light source for high-throughput high-speed Fourier transform spectroscopy (FTS) was pursued by Van der Weide et al. [5-7]. It is based on heterodyne frequency-comb spectroscopy and employs two frequency combs with slightly different

mode spacing. This approach, termed frequency-comb Fourier-transform spectroscopy (c-FTS), relies on expensive mode-locked lasers but enables high-throughput FTS with demonstrated repetition rates of ~ 1 kHz.

2.3.1 Introduction to mode-locked c-FTS

An explanation of c-FTS is provided in the following (for more details see[5]). The method relies on two light sources whose spectra are characterized as frequency combs with slightly different mode spacing. The spacing of the first comb is Δ [Hz], while that of the second comb is Δ+δ [Hz], where *M* is the highest mode number in either of the combs as shown in Figure 2.11(a).

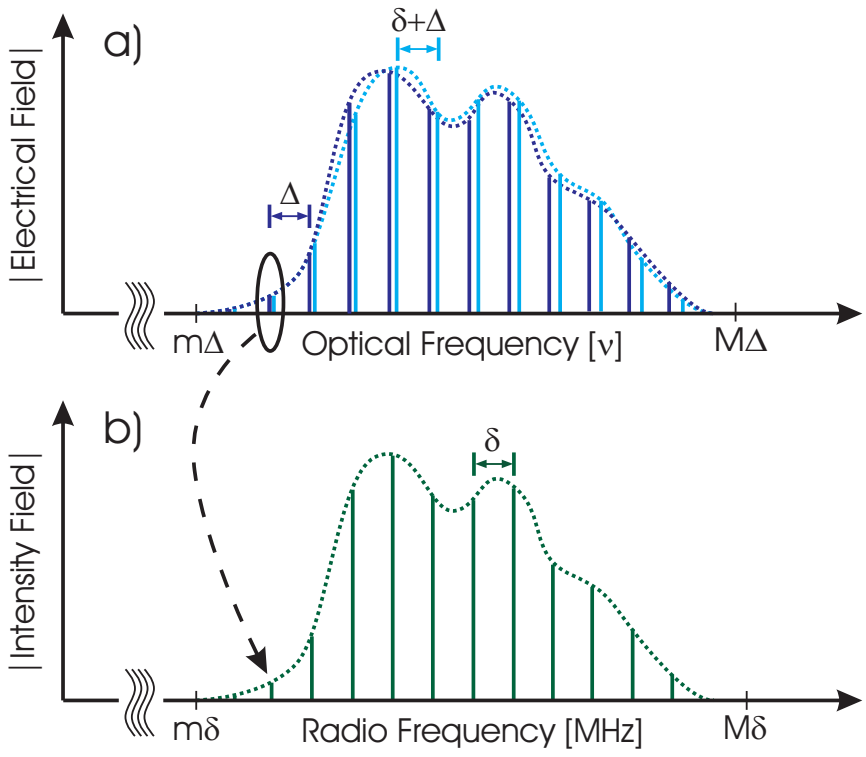

Figure 2.11 Principle of mode locked c-FTS. Interference of two frequency combs where one is slightly detuned by δ (blue and light blue) generates a comb spectrum of much lower frequencies (green).

When overlapping the combs, the time trace of the optical power exhibits variations at various beat frequencies, see Figure 2.11(b). The low-frequency part of this spectrum consists of harmonic beating frequencies $n \cdot \delta$, where $n = m, m + 1, \ldots, M$. The beating amplitude at the harmonics $n \cdot \delta$ is the geometrical mean of the amplitudes at the frequencies $n \cdot \Delta$ and $n \cdot (\Delta+\delta)$. These frequencies both lie very close to each other, and the amplitude of the nth is hence a measure for the amplitude at the frequency $\sim n \cdot \Delta$.

In this way one can monitor the amplitude of high-frequency optical waves (THz to PHz) by monitoring optical beating in a low-frequency range (typically kHz to GHz). In an experiment the time trace of the overlapped frequency combs is detected and the beating spectrum is then inferred from the Fourier transformation of the time trace.

2.3.2 Potentials of c-FTS

A comparison of mode-locked c-FTS with other established hyperspectral light sources is presented in Table 2.1.

The c-FTS spectrometer provides outstanding properties; however, even in this case of mode-locked c-FTS, one has to rely on expensive mode-locked femtosecond lasers and moving cavity mirrors that are needed to increase the repetition rate. To overcome these two drawbacks of mode-locked c-FTS, a variant of the van der Weide et al.'s approach is pursued in this work. Relatively cheap continuous-wave (CW) light sources were used instead of femtosecond pulsed lasers. This method of c-FTS is referred to as CW c-FTS. A major advantage of CW c-FTS is that it does not involve the active control of moving parts like cavity mirrors.

Property	**mode-locked c-FTS**[5]	**Wavelength-agile laser** [30]	**Conventional FTS (FTIR, ...)** [31]	**Scanning grating spectrometer** [32]
Spectral radiance [W/(m^2 Sr GHz)]	10^3	10^3	1	10
Tuning range [octaves]	0.3-10	0.2	1-3	0.1
Accessible spectral range	UV-VIS-IR-THZ	VIS-NIR	UV-VIS- IR	UV-VIS-IR
Maximum Repetition rate [Hz]	10^5	10^5	10^3	10^4
Spectral resolution [GHz]	0.1	10	10	10
Main drawbacks	--	VIS-NIR only	low speed	low throughput or low resolution

Table 2.1 Comparison of hyperspectral light sources. The c-FTS approach offers unique properties that outperform those of other, established techniques. (Color code: excellent, good, mediocre)

2.4 DIFFERENT CW C-FTS DESIGN APPROACHES

In order to conduct comb Fourier transform spectroscopy with continuous-wave light sources, the spectrum of the laser has to be discretized to get the required picket fence structure. A simple way to get a comb structure where no moving parts are involved is to use an either linear or ring cavity. Only certain wavelengths, which are a whole number multiple of the cavity length, are amplified each roundtrip time whereas the rest of the spectrum is

diminished due to destructive interference. Hence, a comb is generated whose structure is dependent on physical cavity length and index of refraction.

The following section presents different c-FTS designs that include CW light sources.

2.4.1 Birefringent cavity

Light propagates through a transparent material by exciting atoms within the medium. Driven by the ***E*** field, electrons reradiate and by so doing generate a refracted wave that moves on. The difference between the frequency of the ***E*** field and the Eigenfrequency of the atoms determines the speed of the wave, and thus the index of refraction. Many crystalline substances are optically anisotropic, that is to say their optical properties are not the same in all directions. An anisotropy in the binding force of atoms results in an anisotropy in the refractive index. A material, which displays two different indices of refraction in the two polarization axes, is said to be birefringent[33].

A hyperspectral light source with a polarization maintaining (PM), birefringent cavity offers two cavity lengths, one for each polarization axis. Because the index of refraction is different in each polarization axis, the two cavity lengths are slightly different. This results in two frequency combs that are slightly detuned, which opens the door to c-FTS.

One potential design of a hyperspectral light source based on a birefringent cavity is shown in Figure 2.12[34]. Here, a ring cavity is formed with a birefringent, Tm-doped, dual clad PM core fiber. The input coupler introduces the pump energy at 793 nm into the outer cladding of the ring. The light from the pump laser partially migrates into the inner cladding where it is

absorbed by the Thulium. The modes of both combs can subsequently beat against each other in the not doped PM fiber that extracts 1% emission at around 1700–1900 nm.

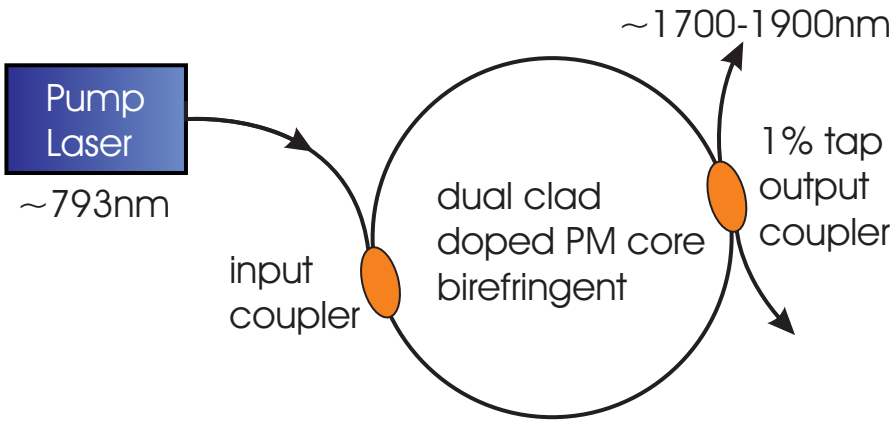

Figure 2.12 Hyperspectral light source based on birefringent ring cavity. The biregringence of the ring cavity results in two cavity lengths, one for each polarization axis. Two comb structures are generated that are slightly detuned and therefore beat against each other to allow CW c-FTS.

One difficulty of this approach is the fabrication of the cavity ring, especially considering the birefringence tailoring and the alignment of the polarization axes when splicing of the two fiber ends. Also, a doped fiber laser does not represent a good inhomogeneous gain medium. Mode competition in the doped fiber laser will degrade the CW c-FTS performance.

The ideal gain medium for multiwavelength lasing will have a very broad inhomogeneous linewidth and a very narrow homogeneous linewidth. A hypothetical example is gas laser containing very hot, very low pressure gas. A linear optical amplifier (LOA) behaves roughly like a *Ne* laser at $4 \cdot 10^9\, K$, $0.001 Torr$. In the following three examples, a LOA will be used for the gain medium in the cavity.

2.4.2 Two CW frequency comb generators

This all-fiber coupled approach also utilizes two slightly detuned frequency combs to allow CW c-FTS. But instead of a birefringent cavity as in the previous design, two CW frequency comb generators are used[34]. Both frequency comb generators include three salient components: A fiber ring cavity, a semiconductor-based linear optical amplifier emitting in the telecommunication range, and an etalon. The etalon selects harmonic frequencies from the amplified spontaneous emission of the linear amplifier and the ring cavity sustains CW lasing at these frequencies. Because the frequency of the modes transmitted by the etalon is temperature tunable, two slightly detuned frequency combs can be generated. For a more thorough analysis and experimental results of this approach, see Chapter 3.

2.4.3 Chirped fiber Bragg grating

A fiber Bragg grating (FBG) is a type of diffraction grating segment of optical fiber where periodically spaced zones in the fiber core are altered to have different refractive indexes slightly higher than the core. This structure selectively reflects a very narrow range of wavelengths while transmitting others. For a chirped fiber Bragg grating, the reflected wavelength, the so called Bragg wavelength, varies with position.

A basic setup that allows c-FTS is depicted in Figure 2.13[34]. A linear cavity is formed by two chirped FBGs and a linear optical amplifier (LOA). Because the Bragg wavelength varies with position in the chirped FBG, the cavity length is no longer constant for all wavelengths but varies discretely with wavelength. For each cavity length, this setup selects harmonic frequencies of the corresponding fundamental cavity frequency from the amplified

spontaneous emission of the LOA and the linear cavity sustains CW lasing at these frequencies.

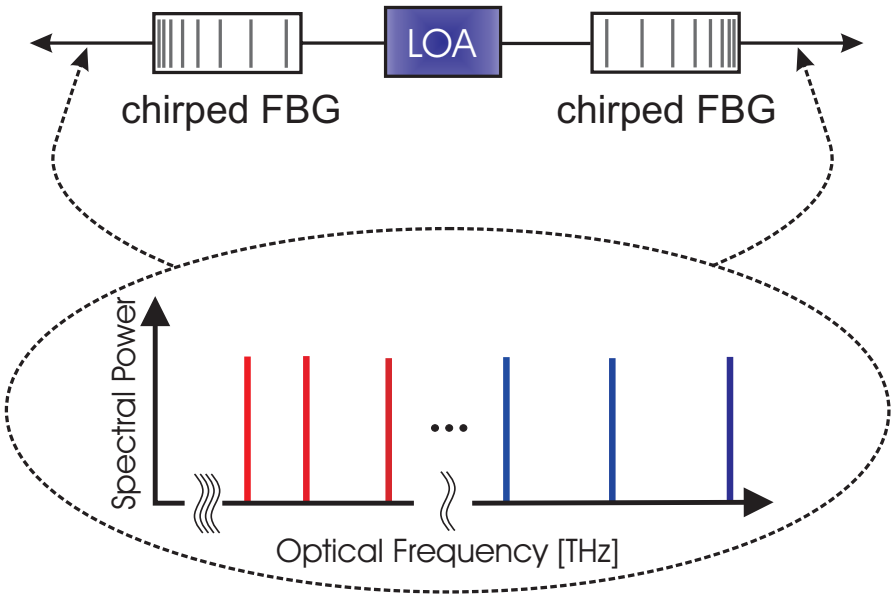

Figure 2.13 Basic setup of c-FTS based on chirped fiber Bragg gratings (FBG). This linear cavity includes multiple cavity lengths because of the variation of the Bragg frequency in the chirped FBGs. Because each cavity length corresponds to a cavity frequency, and because there is no total reflectance in the chirped FBG, the output of this linear cavity can be used for c-FTS.

Each cavity length corresponds to a unique free spectral range (FSR), which makes this approach useful for c-FTS. A part of the frequency comb inside the cavity emerges from each end of the linear cavity as the Bragg wavelengths are not totally reflected in the chirped FBGs.

2.4.4 Highly dispersive cavity

Like the previous design, the salient idea of this method is to generate one optical frequency comb, in which nearby mode pairs beat at unique frequencies. This is achieved with a high dispersion in the cavity. The resonance frequencies are then no longer equally spaced, as in

the case of a vacuum-spaced etalon, but due to the aforementioned dispersion, the spacing of the cavity modes changes as a function of wavelength. Therefore, the interference of adjacent fringes exhibits unique beating frequencies and thus produces a replica of the original comb in the radio frequency range. This approach will be evaluated with simulations and experiments in Chapter 4.

2.5 FEASIBILITY OF CW C-FTS

In this section, feasibility issues like power distribution among the bands or mode competition in the amplifier are considered.

2.5.1 Power considerations

Considering c-FTS, where a replica of a spectrum in the optical frequency range is generated in the radio frequency range, the question arises whether the power of each band in the replica decreases with the number of beating pairs.

An ideal frequency comb consists of equidistant fringes where each fringe has an infinitely small width. Thus each fringe corresponds to only one color, or rather frequency $\omega_i = 2\pi f_i$ where $i = 1, 2, \ldots, N$ and N is the number of lines. The total electrical field of the interference of two slightly detuned frequency combs E_{tot} can be described with

$$E_{tot} = \sum_{i}^{2N} A_i \cos(\omega_i t + \varphi_i) \tag{2.1}$$

where A_i is the amplitude and φ_i the phase of line i. This results in a total intensity field I_{tot}

$$I_{tot} \propto \left(E_{tot}\right)^2 = \left[\sum_{i}^{2N} A_i \cos(\omega_i t + \varphi_i)\right]^2$$

$$= \underbrace{\frac{1}{2}\sum_{i}^{2N} A_i^2}_{DC} + \underbrace{\sum_{i=2}^{2N}\sum_{j=1}^{i-1} A_i A_j \cos\left[(\omega_i - \omega_j)t + \varphi_i - \varphi_j\right]}_{low\ frequency\ beating\ signal} + \underbrace{\frac{1}{2}\sum_{i}^{2N}\sum_{j}^{2N} A_i A_j \cos\left[(\omega_i + \omega_j)t + \varphi_i + \varphi_j\right]}_{high\ frequency\ signal} \tag{2.2}$$

The intensity field consists of a DC component and the two heterodyning signals. The DC component gives the real power of the light source whereas the power of the heterodyning signal is flowing backwards and forwards and can be compared to the 'reactive power' in AC circuit theory. The absolute power of the light source is not a function of *N*, thus assuming constant operating conditions (temperature and current) the DC component is constant. However, with the DC component constant, the number of lines *N* does affect the power of each beating pair $A_i \cdot A_j$ as shown in (2.2).

c-FTS vs. diode laser array

To evaluate the signal power and signal-to-noise ratio, c-FTS can be compared to the laser array approach described in 2.2.3, where every diode laser was encoded at a unique frequency by current modulation.

The intensity of a monochromatic light source with amplitude *A*, wavelength λ, frequency $\omega = 2\pi f$, and phase φ can then be represented as

$$I_{mono} \propto \left(E_{mono}\right)^2 = A^2 \cos^2(\omega t + \varphi) = \frac{1}{2} A^2 \left[1 + \cos\left(2\omega t + 2\varphi\right)\right] \tag{2.3}$$

Modulating (2.3) with a current waveform M

$$M = \frac{1}{2}\left[1+\cos(\omega_{\text{mod}}t)\right] \tag{2.4}$$

where w_{mod} is the modulation frequency. Assuming N diode lasers each modulated at a unique frequency w_{mod_i} results in

$$\begin{aligned} I_{arrayMod} \propto \left(E_{arrayMod}\right)^2 = \sum_i^N I_{\lambda i} \bullet M_i &= \sum_i^N \frac{1}{2} A_i^2 \left[1+\cos\left(2\omega_i t + 2\varphi_i\right)\right] \bullet \frac{1}{2}\left[1+\cos(\omega_{\text{mod}\_i}t)\right] \\ &= \underbrace{\frac{1}{4}\sum_i^N A_i^2}_{DC} + \underbrace{\frac{1}{4}\sum_i^N A_i^2 \cos(\omega_{\text{mod}\_i}t)}_{low\ frequency\ signal} + \\ &\quad + \underbrace{\frac{1}{4}\sum_i^N A_i^2 \cos\left(2\omega_i t + 2\varphi_i\right) + \frac{1}{4}\sum_i^N A_i^2 \cos\left(2\omega_i t + 2\varphi_i\right)\cos(\omega_{\text{mod}\_i}t)}_{high\ frequency\ signal} \end{aligned} \tag{2.5}$$

To compare the efficiency of the diode array approach to c-FTS, now the diode lasers are no longer modulated in current but controlled in such a way that the wavelengths λ_i form a frequency comb where each pair beats at a unique frequency $\omega_i - \omega_j$

$$\begin{aligned} I_{cFTS} \propto \left(E_{cFTS}\right)^2 &= \left[\sum_i^N A_i \cos(\omega_i t + \varphi_i)\right]^2 \\ &= \underbrace{\frac{1}{2}\sum_i^N A_i^2}_{DC} + \underbrace{\sum_{i=2}^N \sum_{j=1}^{i-1} A_i A_j \cos\left[(\omega_i - \omega_j)t + \varphi_i - \varphi_j\right]}_{low\ frequency\ beating\ signal} \\ &\quad + \underbrace{\frac{1}{2}\sum_i^N \sum_j^N A_i A_j \cos\left[(\omega_i + \omega_j)t + \varphi_i + \varphi_j\right]}_{high\ frequency\ signal} \end{aligned} \tag{2.6}$$

For the following evaluation of (2.5) and (2.6), without loss of generality, let it be assumed that $A_i \equiv 1, \forall i \in \mathbb{N}$.

The DC component for the diode array technique in (2.5) is only half of the DC signal for c-FTS. This is because the current modulation turns the diode lasers on and off, the lasers are 'blinking', and therefore the absolute power is decreased by 50%. Looking at the information carrying low frequency signals, the power of each band is four times bigger in the c-FTS case compared to the diode laser array approach.

Although this comparison is more of hypothetical nature due to the infeasibility of operating scores of monochromatic diode lasers, it shows that c-FTS has a big advantage over the diode laser array approach with a four times bigger signal power per band.

c-FTS conducted with broadband light sources

If the comb structure is generated with a single broadband light source, the absolute power constraint of course still holds, namely that the output power of the laser (DC signal in (2.2)) is constant for constant operating conditions and not a function of the number of lines of the comb. Thus the more lines there are in the lasing spectrum of the source, the smaller the amplitudes A_i and hence the smaller the signal power per band of the beating signal. This shows a trade-off between number of bands, or rather spectral resolution, and signal power per band.

2.5.2 Mode competition

When generating a frequency comb with an amplifier inside the cavity, the question arises whether mode competition in the amplifier causes instability of the comb structure. In other words: What is the smallest frequency difference between two fringes in a comb before they start to have an affect on each other and thus make c-FTS impossible?

To answer this question, two narrow band lasers and a linear optical amplifier (LOA) were set up as shown in Figure 2.14. The salient idea was to modulate the amplitude of laser 1 and amplify both lasers with the LOA. As both lasers were competing for the gain of the LOA, the amplitude modulation of laser 1 was also modulating the amplitude of laser 2. When laser 1 was strong, a less amplification for laser 2 was observed, indicating that the potential for cross talk exists. By decreasing the wavelength difference between the two spectra, the amplitude of the oscillation of laser 2 at the modulation frequency was a measure for the mode competition in the LOA.

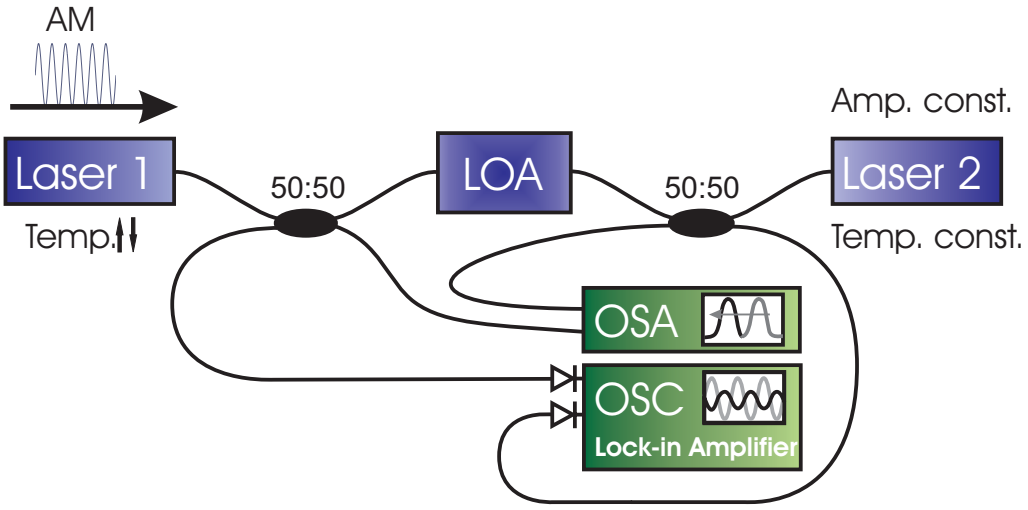

Figure 2.14 Experimental setup. Laser 1 was amplitude-modulated at 10 kHz. The temperature of laser 1 was controlled with a sawtooth waveform at 10 Hz in such a way that the spectrum of laser 1 passed the constant spectrum of laser 2 two times per period. The data acquisition system consisted of an optical spectrum analyzer (OSA) and an oscilloscope (OSC) in combination with a lock-in amplifier.

Data recorded with the OSA is presented in Figure 2.15. Laser 1 was only half as bright as laser 2 because of the amplitude modulation, that is to say laser 1 was “blinking”. The

spectrum of laser 1 was captured at the minimum (green) and at the maximum temperature (blue) applied.

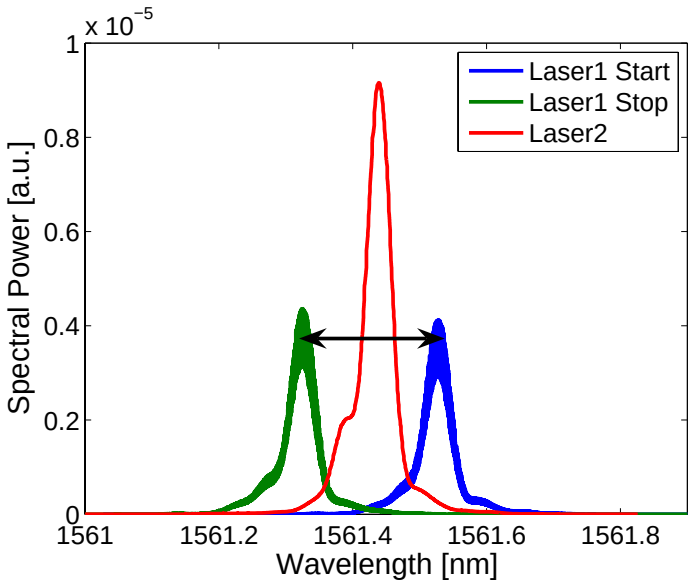

Figure 2.15 OSA data of current and temperature modulated laser 1 and constant laser 2. Due to the temperature modulation, the wavelength difference between the two spectra is changed continuously.

The effect of the gain competition in the LOA can be seen in Figure 2.16. The amplitude modulation of laser 1 affected both lasers, because they competed for the same gain in the LOA. The amplitude of the modulation is stronger for the "actively" modulated laser 1.

A lock-in amplifier was used to record the power of laser 2 at the modulation frequency. Assuming there was mode competition in the LOA, a peak for the signal power of laser 2 at the modulation frequency was expected, when the two spectra were overlapping. However, as the wavelength difference between the spectra of the two lasers was changed through temperature control of laser 1, the modulation power of laser 2 changed only slightly because of the brighter lasing operation due to the lower temperature of laser 1. Although, the

bandwidth of the lock-in amplifier was relatively fast compared to the temperature controlled change of the spectral shape, no peak of the modulation power of laser 2 could be observed.

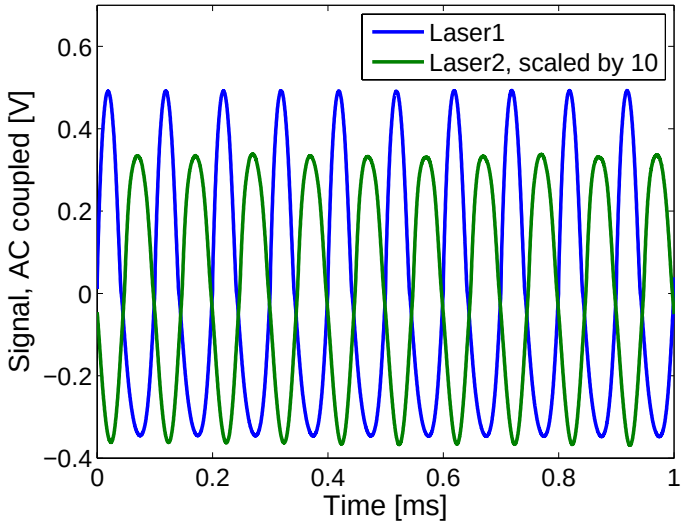

Figure 2.16 Time trace of laser 1 and laser 2 recorded with the oscilloscope. Both lasers are competing for gain in the LOA. AC coupled detectors were used because of the strong DC component of the signals. Considering the scaling of the trace of laser 2, the modulation of has a bigger effect on laser 1 ('active') than on laser 2 ('passive').

According to the results of this experiment, mode competition problems should be decoupled from the mode spacing in the frequency combs chosen for CW c-FTS. This conclusion agrees with the results from Qureshi et al.[35]. In this paper, a different setup was used including an amplifier and a fiber Bragg grating. It was also shown that a lower mode competition and an overall higher stability of the frequency comb can be achieved for a linear optical amplifier compared to a semiconductor optical amplifier (SOA).

CHAPTER 3. DEVELOPMENT OF A CW C-FTS LASER BASED ON BEATING OF TWO FREQUENCY COMBS

Time- as well as frequency based simulation results of the interference of two CW frequency combs will be given in the first section of this chapter, whereas the second and third section will present the experimental setup and results. A conclusion will sum-up the pros and cons of this approach and close this chapter.

3.1 INTRODUCTION

The work in this chapter[34, 36] presents a variant of Van der Weide's et al. [5-7] approach to mode locked comb Fourier transform spectroscopy (c-FTS). Their work employed two expensive mode-locked lasers but enabled high-throughput c-FTS with demonstrated repetition rates of ~ 1 kHz. However, mode locked c-FTS still relies on moving cavity mirrors to obtain interferograms at a sufficiently high duty cycle. The variant of mode locked c-FTS that will be presented in this chapter shows that heterodyne frequency comb spectroscopy can be conducted with inexpensive and technically simple continuous-wave (CW) frequency comb generators. This method will be referred to as CW c-FTS. A major advantage of this approach is that it relies on an all-fiber laser design and does not involve the active control of moving parts such as cavity mirrors.

3.2 SIMULATIONS

Continuous-wave c-FTS had not been presented to the optical research community before work on this thesis was conducted. Therefore, extensive simulations of CW c-FTS were necessary to assure a theoretical feasibility of CW c-FTS.

3.2.1 Uncertainties in the CW c-FTS understanding

Below, some questions will be listed that needed to be answered through simulations to come up with a promising experimental setup.

- One major difference between CW c-FTS and mode locked c-FTS as it was presented in 2.3 is that the length of the CW ring cavity is significantly longer compared to the cavity length of a mode-locked laser. Rings that are too small cause low gain and high bend losses. What are the effects of longer cavity lengths and thus, of shorter free spectral ranges of the cavities on the performance of CW c-FTS?

- How to detune the two combs in the CW c-FTS setup? Van der Weide et al. showed that cavity frequency detuning of ~100 Hz can be achieved for mode locked c-FTS[5]. Considering a setup with two ring cavities and no moving parts, the difference in the two cavity frequencies might be a lot bigger. What are the ramifications?

- Whereas all phases of the cavity modes were aligned in mode locked c-FTS, are there negative effects due to the random phases in the CW setup?

These questions will be answered in the following section, which is divided into two parts that are presented in an ascending complexity order: The first part shows a frequency domain based analysis, which takes the comb structure for granted and thus gives an opportunity for a quick spectral analysis. The second part goes back to the time domain, calculates the electrical fields of the two combs and then computes the FFT of the output intensity time trace. In addition to the questions listed above, it has to be answered, whether or not these two different types of simulations converge.

3.2.2 Frequency based spectral analysis

This spectral analysis evaluates the dependency of input parameters (spectral coverage, spectral resolution, and repetition rate) on the feasibility of two resulting combs for CW c-FTS. Two basic ring cavities, each only including a linear optical amplifier (LOA), were considered. According to the desired design parameters and with respect to the wavelength coverage of a LOA, the input parameters were chosen as follows:

- Wavelength coverage: 1500–1600 nm → Δf = 125 THz
- Spectral resolution: ν_{res} = 0.05 cm^{-1}
- Repetition rate: t_{rep} = 20 μs

A simplified proceeding of the spectral analysis is given in the following:

Not taking the approximate channel bandwidth $f_{BW} = \frac{1}{2\pi t_{rep}}$ into account, half of the spectral resolution (mode spacing of the frequency comb) can be used for CW c-FTS. If the frequency difference between a beating pair is bigger than half of the mode spacing, beating with the consecutive mode would result in an ambiguous replica. Therefore, the most efficient setup of the two combs is achieved when the difference of the first beating pair in the wavelength coverage is the channel bandwidth f_{BW}

$$\Delta f_{beat\,\min} = f_{cavity2} - f_{cavity1} \stackrel{!}{=} f_{BW} \tag{3.1}$$

and the difference of the last beating pair is

$$\Delta f_{beat\max} \stackrel{!}{=} \frac{1}{2}\nu_{res} \approx \delta n = \delta \frac{\Delta f}{\nu_{res}} \tag{3.2}$$

where n is the integer number of beating pairs in the wavelength coverage of the amplifier. The difference of the cavity frequencies of both ring lasers δ can be found with (3.2), which yields the mode spacing of the second cavity: $\nu_{res} + \delta$. With the mode spacing and the index of refraction of the cavities known, the effective length of both cavities can be found.

The first constraint (3.1) can be met by using mode wraps. Mode wraps occur when $m\delta > \nu_{res}$ where m is the highest mode number of the spectral coverage of the amplifier. In other words, by making the two effective ring cavity lengths unequal, it can happen that the two resulting combs diverge fast enough that one comb is passing the other comb. This passing of modes will be referred in this thesis as mode wraps.

A visual result of the spectral analysis with the input parameters given above is presented in Figure 3.1. The two blue lines mark the spectral coverage of the amplifier. The inset zoom shows 6 out of 8333 beating pairs in the wavelength range of operation of the LOA. The orange line shows the frequency difference between beating pairs and thus indicates a mode wrap at each trailing edge of the saw-tooth waveform.

The cavity length for ring laser 1 was found to be 0.13605… m. Taking into account that the ring has to include at least an amplifier and some sort of output coupler, the short cavity length obtained in the analysis is not feasible. Also, such short rings cause low gain and high bend losses. In addition, the ring cavity lengths showed a mismatch of 7.619… μm. An experimental setup of two rings where the mismatch is either achieved by different lengths of

the fiber used in the cavity of by controlling the ambient temperature of both ring lasers would be very challenging.

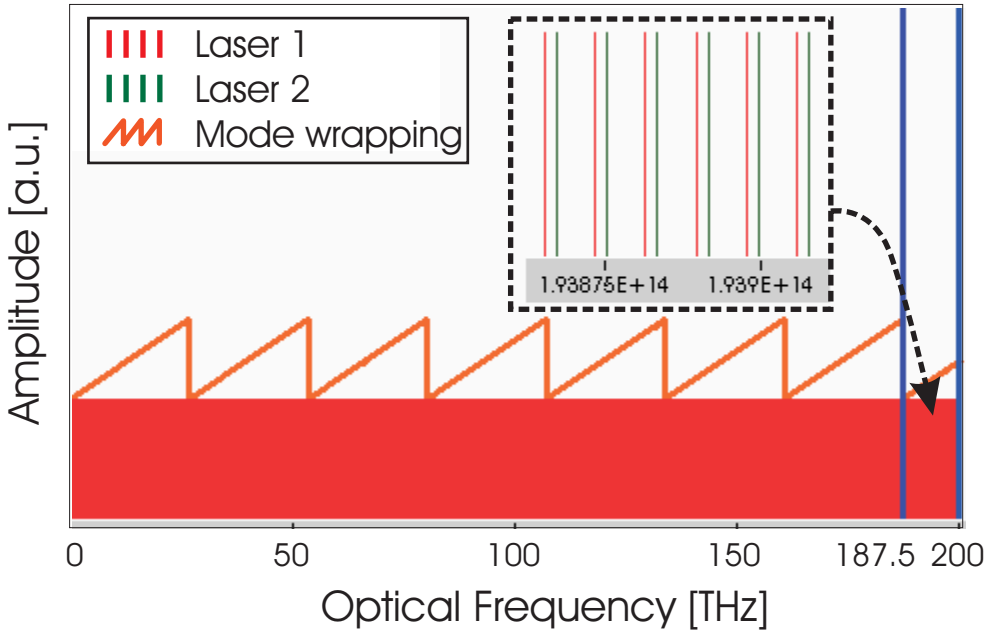

Figure 3.1 Spectral analysis of two beating combs generated in two ring lasers. The two blue lines indicate the assumed spectrum of the LOA (1500-1600 nm). The cavity lengths were found in such a way that the first beating pair of the spectrum of the LOA has a frequency difference of $\delta \approx 8$ kHz and that the two modes of the last beating pair are about half of the mode spacing of laser 1 apart.

In order to avoid these design challenges, a setup with two ring lasers was chosen with rather long cavity lengths (~100 m) that both include an etalon, which results in a 'cavity inside a cavity' setup. The two etalons can be temperature controlled, in order to obtain the necessary detuning of the cavity frequency.

3.2.3 Algebraic time based analysis

The frequency based simulation of two beating frequency combs presented above gives a quick spectral analysis that helps to design the CW c-FTS hyperspectral light source.

However, it does not simulate how the frequency combs are generated. This algebraic analysis goes back to the electrical field ***E*** and intensity field ***I*** of the ring cavity in the time domain. The purpose of the algebraic analysis is not to solve design problems like the spectral analysis, but rather to help understand the physics behind the frequency comb generation in ring cavities.

The ***E*** field of a ring laser is found to be

$$E_{ring} = \sum_{i}^{N} A_i \cos(2\pi f_c t + \varphi_i) \tag{3.3}$$

where f_c is the cavity frequency, A_i the amplitude and φ_i the phase of mode i, and N the number of modes. The ***E*** field of two ring lasers, where one cavity frequency is slightly detuned by δ is then

$$E_{12} = E_{ring1} + E_{ring2} = \sum_{i}^{N} A_i \cos(2\pi f_c t + \varphi_i) + \sum_{j}^{M} B_j \cos\left(2\pi (f_c + \delta) t + \varphi_j\right) \tag{3.4}$$

which results in an ***I*** field

$$I_{12} \propto \left(E_{ring1} + E_{ring2}\right)^2 = \left[\sum_{i}^{N+MW} A_i \cos(2\pi f_c t + \varphi_i) + \sum_{j}^{N} B_j \cos\left(2\pi (f_c + \delta) t + \varphi_j\right)\right]^2 \tag{3.5}$$

where *MW* is the number of mode wraps that occur up to the highest frequency of the amplifier lasing spectrum.

It was shown in 2.5.1 that this intensity field can be decomposed into a DC component, a high frequency signal and low frequency beating signal. Note here that the following equation represents an output intensity of the two beating frequency combs. Thus, only the

beating pairs that reside in the lasing spectrum of the amplifier are considered because there is no measurable emission above or below these colors. The number of modes of each ring cavity that reside in the lasing spectrum of the amplifier is represented by M.

$$I_{12out} \propto \underbrace{\frac{1}{2}\sum_{i}^{2M} A_i B_i}_{DC} + \underbrace{\sum_{i=2}^{2M}\sum_{j=1}^{i-1} A_i B_j \cos\left[(\omega_i - \omega_j)t + \varphi_i - \varphi_j\right]}_{low\ frequency\ beating\ signal} + \underbrace{\frac{1}{2}\sum_{i}^{2M}\sum_{j}^{2M} A_i B_j \cos\left[(\omega_i + \omega_j)t + \varphi_i + \varphi_j\right]}_{high\ frequency\ signal} \tag{3.6}$$

A fast Fourier transformation (FFT) of the time trace of the intensity output (3.6) can be used to evaluate the effect of the random phases in the $\boldsymbol{E}$ field φ_i or of noise from the data acquisition (DAQ) system on the performance of CW c-FTS.

Parameter setting

Because the native frequencies of the cavity modes reside in the THz–PHz range but due to beating, a replica of the spectrum is generated in the radio frequency range, using the parameter set obtained in the spectral analysis above turned out no to be feasible considering the available hardware resources. This huge dynamic range sets high demands on both time- as well as frequency resolution. For the time resolution, a rule of thumb is that the sample frequency has to be about ten times faster than the highest frequency to be simulated in order to capture the dynamics of the system. At the same time, the frequency resolution has to be high enough to resolve all the frequency components. For the spectral analysis results above, that would result in 40G samples for the simulation of one cavity mode. Because the computational resources could not cope with such an amount of data, the parameter set had to

be changed. Fortunately, an unrealistic parameter set is not a big drawback for the algebraic analysis because its purpose is not to find the right design parameters but to answer general questions about continuous-wave heterodyning.

The spectral analysis was used to find a parameter set for the algebraic simulation that met both time- and frequency resolution demands of the generated system. The parameter set for the algebraic, time based analysis is given in Table 3.1.

Modified Spectral Analysis		**Algebraic Analysis**	
λ_{min} of laser emission	1 m	Sample Frequency	3 GHz
λ_{max} of laser emission	1.05 m	Simulation Time	1 ms
Cavity frequency of ring 1	600 kHz	Amplitude of all cavity modes A_i	1 a.u.
δ, cavity detuning	12.9 kHz		
Repetition rate	20 μs	Phase of all cavity modes φ_i	random [0 2π]
Spectral resolution	$2 \cdot 10^{-5}$ cm^{-1}		
Number of Beating Pairs	23	→ Frequency Res.	1 kHz

Table 3.1 Parameter set for time based algebraic simulation of two interfering frequency combs.

To ease the time resolution demands, the operating wavelength range of the amplifier was significantly shifted towards lower frequencies. This however does not falsify the simulation results because the beating signal still resides in a realistic range and the chosen sample frequency is within the bandwidth of a commercially available DAQ system.

The simulations results are presented in Figure 3.2. The top plot shows DC component, the beating- and the high frequency signal of the output intensity of the two beating frequency combs. The beating signal was found to be composed of exactly 23 beating pairs, as expected.

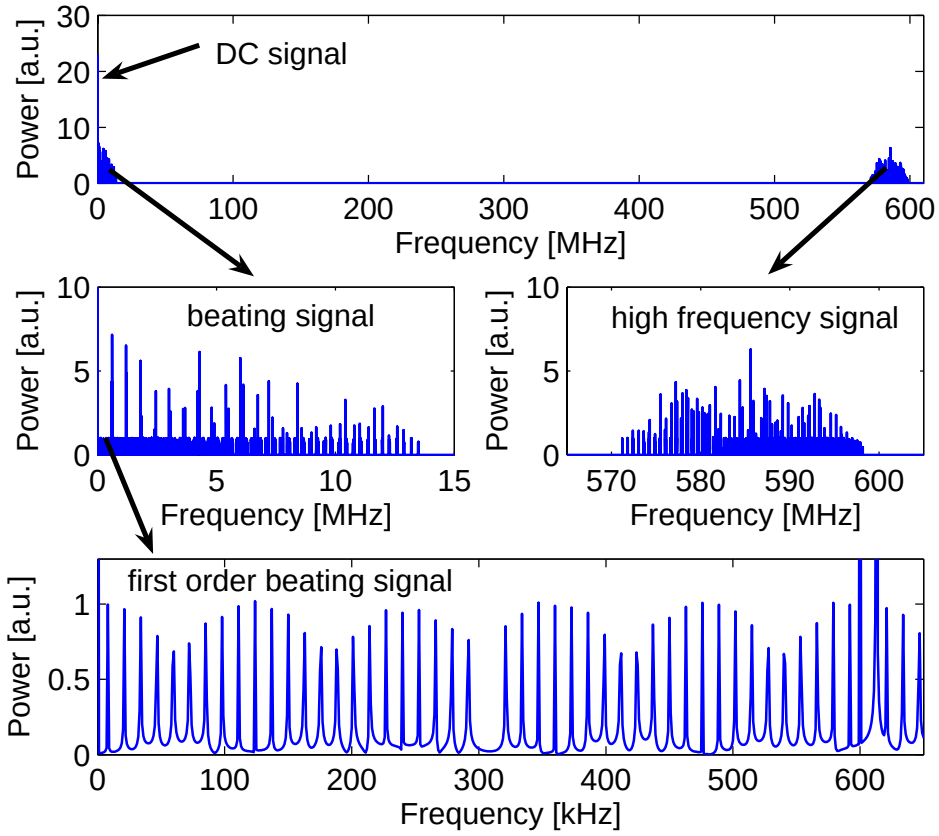

Figure 3.2 Simulation results of two slightly detuned frequency combs. The DC signal and the two heterodyning components can be clearly seen in the top plot. Only the first small section of the beating signal shows the beating of the 23 simulated beating pairs from about 0-300 kHz. The beating signal above 300 kHz is due to higher order beating where not consecutive modes interfere.

A closer look at the beating signal in (3.6) shows that all possible pairs of modes of the two frequency combs are included. In this work, the beating of adjacent modes will be referred to as "first order" beating to distinguish this replica from "higher order" beating. For each

higher order beating, the number of beating pairs in the replica decreases by 1. Thus, in this case of only 23 beating pairs for the first order beating, the footprint of higher orders gets rapidly smaller.

The highest order is 23 with the information of only one beating pair. The bottom plot in Figure 3.2 shows the first order beating. The amplitudes of the 23 picket fences are not exactly 1 because of the frequency discretization in the FFT. The amplitude is close to 1 when the frequency difference between the corresponding beating pair is close to a frequency discretization point in the FFT ($k \cdot \Delta f = k \cdot 1kHz, k \in \mathbb{N}$). Because the frequency difference between two fringes of the beating signal and the frequency resolution of the FFT are constant (δ and Δf), the amplitude of the beating signal oscillates.

The bottom plot in Figure 3.2 also confirms the results of the spectral analysis. The beating of the first frequency pair resides at ~ 8 kHz, the channel bandwidth of the measurement. Also, almost half of the mode spacing is used by the first order beating (~300 kHz).

3.2.4 Conclusions

In 3.2.1 some questions regarding uncertainties in the understanding of CW c-FTS were listed. With the results of the spectral and the algebraic analysis, these questions can be answered.

- Compared to mode-locked c-FTS, what are the effects of longer cavity lengths and of a stronger detuning of the two cavities on the performance of CW c-FTS?

  A longer cavity length and thus a smaller free spectral range of the ring laser and a bigger difference δ between the mode spacing of the two cavities bring forth mode

wraps. Mode wraps occur when the two combs are diverging so fast that one comb is passing the other comb.

- Whereas all phases of the cavity modes were aligned in mode locked c-FTS, are there negative effects due to the random phases in CW c-FTS?

  The output intensity of the two interfering frequency combs (3.6) and the bottom plot in Figure 3.2 that displays the first order beating signal do not show any negative effects of random phase of the modes in the two cavities on the performance of CW c-FTS.

3.3 EXPERIMENT

With the positive conclusions from the simulations, a CW light source was implemented. Two all-fiber frequency comb generators were combined to produce interlaced continuous-wave frequency combs with a maximum mode detuning of 25 GHz ± 10 MHz. These combs were used to demonstrate the feasibility of continuous-wave frequency comb Fourier transform spectroscopy.

The next two sections will show the setup and the results of the experiment.

3.3.1 Setup

The experimental apparatus for the CW c-FTS light source is depicted in Figure 3.3. Two slightly detuned frequency combs were generated in two separated ring cavities. In Figure 3.3a) the details of a frequency comb generator are displayed. The layout is based on the work reported by Qureshi et al.[35]. It consists of three salient components: A fiber ring cavity, a semiconductor-based linear optical amplifier ((Finisar/Genoa G111[37]) emitting in the

telecommunication range and an etalon (Micron Optics FFP-I, finesse: 40, mode spacing: 25 GHz).

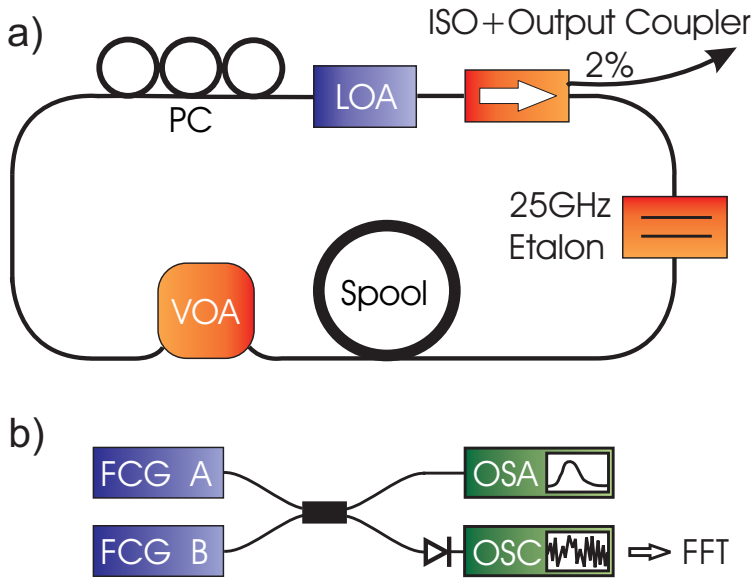

Figure 3.3 Schematic of the experimental setup. a) Layout of the frequency-comb generator (FCG). *LOA:* linear optical amplifier; *PMC*: Polarization maintaining control; *VOA:* variable optical attenuator; ISO: optical isolator. b) Overall setup. The output from two frequency generators (FCG A and B) is combined and the time trace of the optical power is recorded with a photo-receiver and an oscilloscope (OSC). The output can be spectrally analyzed with an optical spectrum analyzer (OSA).

The etalon selects harmonic frequencies from the amplified spontaneous emission of the linear amplifier and the ring cavity sustains CW lasing at these frequencies. The cavity also contained a variable optical attenuator (JDS Uniphase MV47W) that was used to control the gain in the cavity and thus the output power of the comb generator. Other elements were a polarization controller (Fiber Control FPC) for maintaining a linear polarization in the mode cavity, and an optical isolator (AOC Tap-WDM-Isolator Hybrid) that guaranteed unidirectional lasing operation. The frequency of the modes transmitted by the etalon was

temperature tunable by ~300 kHz/K. The length of the ring cavity was chosen so that several cavity modes reside within a mode submitted by the etalon.

Optical power was subtracted from the cavity by a 2% output coupler (integrated into the isolator). As shown in Figure 3.3b) the output from two comb generators was combined and the optical power of this combination was then monitored with a data acquisition system consisting of a photo receiver (New Focus MV47W) and a real-time sampling oscilloscope (Tektronix TDS7404; 4 GHz bandwidth, 20 GSample/s). The time trace recorded with this device (400 μs) was then Fourier transformed. The output could also be recorded with an optical spectrum analyzer (OSA; Agilent 86142B, ~ 8 GHz resolution).

A picture of the experimental setup is presented in Figure 3.4. Both frequency comb generators were built into a fiber optic patch panel (dfbFiber).

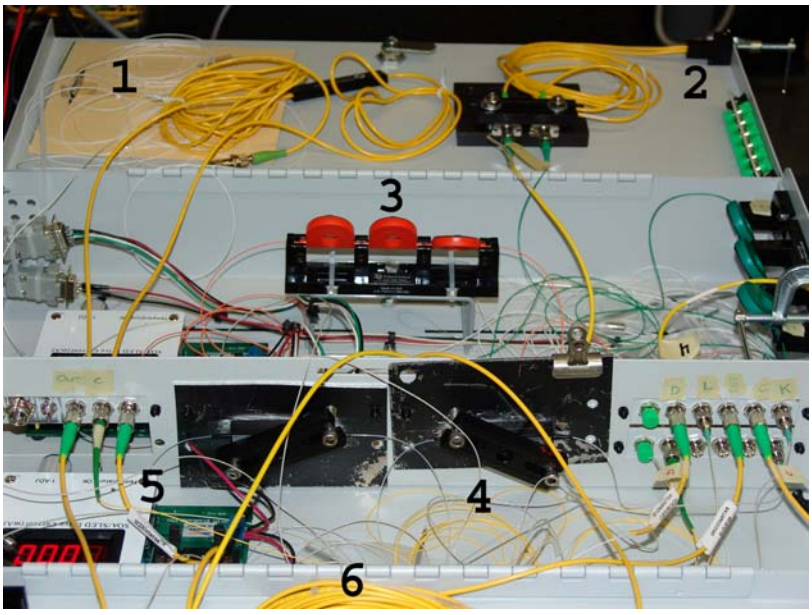

Figure 3.4 Picture of experimental setup. (1) Optical isolator + output coupler; (2) Variable optical attenuator; (3) Polarization controller; (4) 25 GHz etalon; (5) Linear optical amplifier and driver board; (6) Fiber spool

3.3.2 Results

The results from the experiments are shown in Figure 3.5. Figure 3.5a) displays the spectra of both combs. An insert in this Figure show zooms in on the top of the spectrum. The individual cavity modes can be discerned. Each spectrum consists of ~ 100 modes with 25-GHz spacing. Figure 3.5c) shows the Fourier transformation of the time trace recorded, both for a single comb and for combined combs. One clearly sees a strong contribution below 300 MHz for both cases. The strong peak at 2.5 GHz is an artifact caused by the data acquisition system. This contribution is caused by optical beating of the cavity modes (spacing ~ 5 MHz) within all modes transmitted by the etalon (width < 600 MHz). The low-frequency component is also prevalent in the combined output, and there is a second component around 2-4 GHz. This contribution stems from the mutual optical beating of the closely spaced comb modes in comb A and B. This was confirmed by temperature-tuning of the etalon in one comb generator, which changed the mode frequency, and by observing a shift of the center frequency of the mutual beating spectrum over the whole frequency range in Figure 3.5c). Since the etalon modes in both lasers are rather broad the mutual beating spectrum appears to be smeared out rather than exhibiting a fence of beating frequencies as expected from the above theory. For a setup with a larger detection bandwidth it would be possible to increase δ and to discern individual cavity modes in the mutual beating spectrum.

That this experimental apparatus indeed constitutes a spectrometer is demonstrated in Figure 3.5b) and Figure 3.5d). By adjusting the polarization control and the gain in the cavity the output of both comb generators was red shifted over 100 etalon modes (~ 2.5 THz) and the detuning δ of both cavities was ~ 10 MHz. From the above theory of c-FTS one would

expect the mutual beating spectrum to shift 100 x 10 MHz = 1 GHz toward lower frequency, which agrees very well with the result in Figure 3.5d).

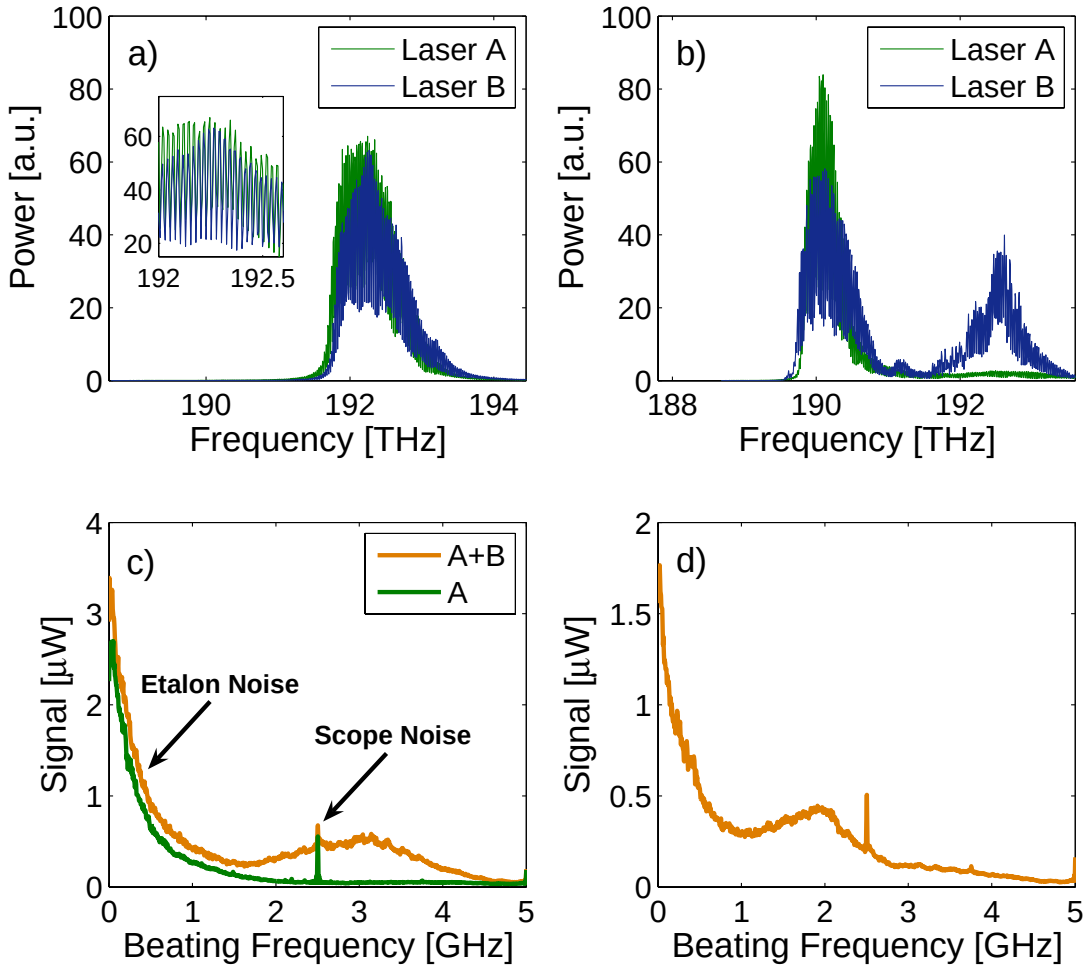

Figure 3.5 Spectra and Fourier transformation of the output of the frequency comb generators. a) Spectra from both cavities recorded with the OSA. An inset zoom reveals the etalon modes, spaced by 25 GHz. The detuning of the cavities by ~ 3 GHz at 192 THz was too small to be resolved by the OSA. b) Same as in (a), however, the frequency combs are red-shifted by ~ 2.5 THz. c) Fourier transformation of time traces generated by the frequency combs in (a), both for an individual comb and for the combination of both. d) Fourier transformation of the time traces generated by the combination of the frequency combs in (b).

3.4 CONCLUSION

The feasibility of CW c-FTS was shown, for which two frequency comb generators were assembled. The mode spacing and center frequency of each comb could be adjusted individually by temperature control of the two 25 GHz etalons and polarization control of the two ring cavities.

However, especially the spectral resolution but also the measurement repetition frequency achieved in this experiment were both not sufficiently high to meet the demands of a hyperspectral light source set by e.g. mode locked c-FTS in Table 2.1. In particular the finesse of the cavity modes has to be improved to enhance the frequency resolution of the CW c-FTS signal. Although mode competition in the amplifier should not have a significant, negative effect on the performance of CW c-FTS, the setup of relying on a secondary filter within the ring laser might have contributed some noise to the CW c-FTS signal. A different setup with only one cavity in the laser ring will decrease the noise due to mode competition and therefore allow higher measurement repetitions rates than the presented 2 kHz.

A hyperspectral laser, where only one ring cavity generates an unequally spaced frequency comb to allow CW c-FTS, will be presented in the next chapter.

CHAPTER 4. DEVELOPMENT OF CW C-FTS SOURCE BASED ON SINGLE COMB BEATING

This chapter presents a new approach to CW c-FTS where only one cavity inside the laser ring generates a unequally spaced frequency comb. In addition to the benefits of conventional FTS (broad spectral coverage, high throughput) this technique does not involve moving parts, offers high repetition rates and a good signal-to-noise ratio (SNR) due to high spectral radiance sources. It has the potential for unlimited spectral resolution, all in an inexpensive and fiber-coupled arrangement[34, 38].

4.1 INTRODUCTION

The salient idea of this method is to generate one optical frequency comb, in which nearby mode pairs beat at unique frequencies. This beating causes a frequency downshift of the infrared spectrum from native frequencies in the PHz domain into the radio-frequency (RF) range, where the beat spectrum resides. The RF spectrum is a replica of the actual spectrum and can be obtained simply by a fast Fourier transformation (FFT) of the time domain signal.

An unequally frequency comb can be generated by including a highly dispersive element in a fiber ring laser. Beating of nearby modes in the comb naturally assigns unique amplitude modulation frequencies to each spectral component emitted. A simplified output comb of the ring cavity consisting of m fringes is outlined in Figure 4.1a). The resonance frequencies are not equally spaced, as in the case of an etalon, but due to the aforementioned dispersion, the spacing of the cavity modes changes as a function of wavelength. Therefore, as required for this approach, the interference of adjacent fringes exhibits unique beating frequencies A_i and

thus produces a first order replica of the original comb in the RF range (see Figure 4.1b)). Furthermore, high order replicas emerge from interference of nearby (but not adjacent) fringes, e.g. second order beating frequencies B_i.

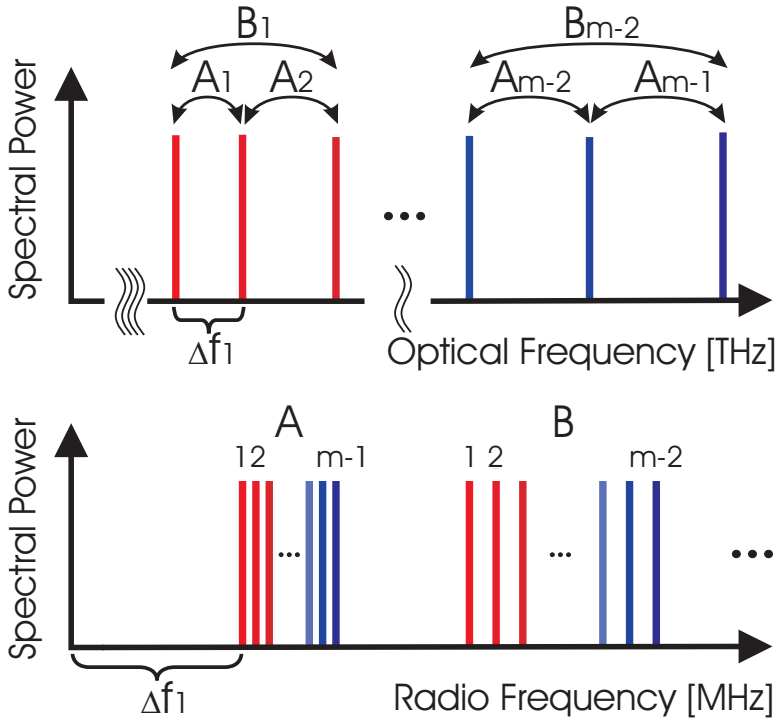

Figure 4.1 Beating of the frequency comb. (a) Sketch of the output comb consisting of *m* fringes. The fringes are not equally spaced, because of the high dispersion in the cavity; thus, adjacent fringes interfere at unique frequencies A_i. Beating also occurs in higher orders, e.g. the second order beating frequencies B_i. (b) First and second order replicas of the optical frequency comb in the radio frequency range.

Using high orders entails a coarser discretization but because of the diverging structure of the output comb of the cavity, the footprint in the Fourier space becomes larger in higher orders. Also, because the full width half max (FWHM) of each mode does not change when the mode is used in higher order, the effective finesse scales approximately with the order number.

Additional advantages of high orders are the decrease of inherent semiconductor amplifier intensity noise associated with the higher frequencies and the possibility of averaging multiple orders. The maximum order number is set when the information in two consecutive orders starts to overlap.

4.2 SIMULATIONS AND BASIC EXPERIMENTS

Although simulations regarding optical interference of frequency combs were already made in 3.2, more simulations were necessary for two reasons. Firstly, to understand the physical properties of the dispersive element, the grating compressor; and secondly, because the conditions regarding optical beating changed from the two combs setup to the case, which is discussed in this chapter, where only one unequally spaced frequency comb allows CW c-FTS.

4.2.1 Grating compressor design

The grating compressor design is based on work from Treacy[8]. Treacy developed the theory of the diffraction grating pair and showed that the time delay in a diffraction grating pair varies with frequency because the length of the ray path is different for different wavelengths.

A grating compressor is obtained by a combination of two diffraction grating pairs as depicted in Figure 4.2. Note that λ_1 and λ_2 have different path lengths through the compressor.

When polychromatic light is directed at a diffraction grating, it is reflected as a sheet. The waves spread out into the sheet according to wavelength. To optimize the setup for given

basic conditions, like grating properties and spectral coverage of the linear optical amplifier, the setup was designed for a spectral coverage of 1530–1570 nm in a way that the entire width of gratings *G2* and *G3* was illuminated.

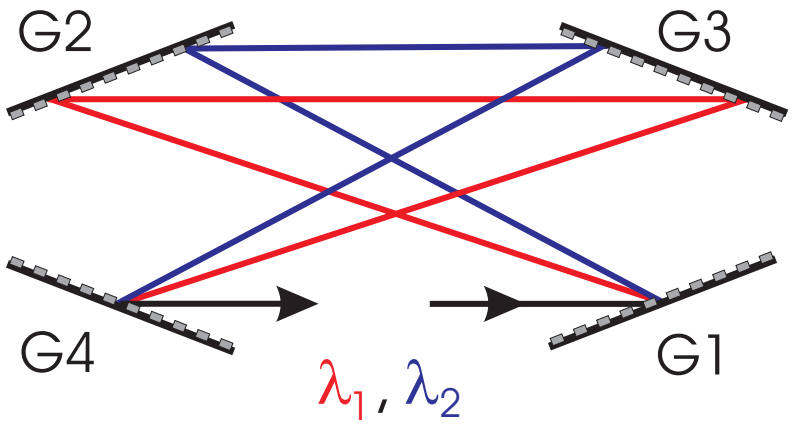

Figure 4.2 General setup of a grating compressor consisting of two diffraction grating pairs.

To evaluate where the first order replica of the spectrum in the optical frequency range was to be expected, a computer model of a ring cavity including a grating compressor was implemented. The dependency of effective path length as a function of wavelength was obtained and with

$$\frac{\Delta f}{f} = \frac{\Delta \lambda}{\lambda} \tag{4.1}$$

the change in free spectral range over the spectral range 1530–1570 nm could be found. The results of the simulations are presented in Figure 4.3. The beating of around 90.000 modes in the cavity generates a first order replica at 47–62.5 MHz.

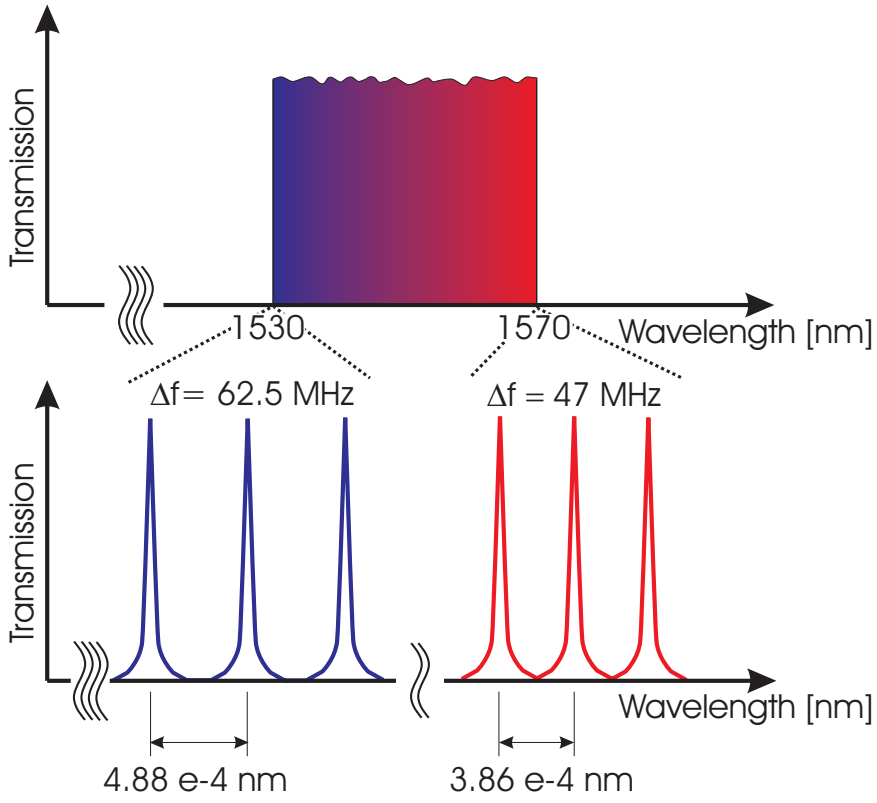

Figure 4.3 Simulation results of a ring cavity including a grating compressor. Beating of the unequally spaced frequency comb results in first order replica at 47–62.5 MHz.

However, the math implemented in the computer model of the grating compressor assumed an infinite resolving power of the gratings. The resolving power R of a diffraction grating can be expressed as[33]

$$R = \frac{\lambda}{\Delta\lambda} = m \cdot N \tag{4.2}$$

where $\Delta\lambda$ is the least resolvable wavelength difference, m is the order of diffraction, and N is the number of grooves covered with the incoming light beam. Because only one polychromatic ray strikes *G1* and *G4* in the grating compressor, the resolving power of the gratings will certainly reduce the simulated performance of the intra-cavity grating

compressor due to less dispersion. As a result, the modes in a real cavity were expected to have a larger FSR with a smaller relative variation over wavelength.

To prove that assumption, a fiber ring cavity of known length was fed with a current modulated monochromatic light source (~1531 nm) and the output was monitored with an oscilloscope. The FSR of this ring cavity with known length L could be calculated to

$$FSR = \frac{c}{n \cdot L} \tag{4.3}$$

where c is the speed of light in vacuum and n the refraction index of the fiber. Then the grating compressor as presented in Figure 4.2 was included in the ring cavity and the traces on the oscilloscope of the two setups were compared. With (4.3) and the two numbers of fringes per modulation cycle for both setups, the FSR of the ring cavity including the grating compressor could be found for wavelengths close to the monochromatic light source.

This whole process was redone with a different monochromatic light source (~1562 nm) and although the parameters of the simulation were set as close to this experiment as possible, the results of the simulation presented in Figure 4.3 could not be reproduced. Whereas the first order replica was simulated at 47–62.5 MHz, the measured one was at around 190.7–214.2 MHz. This change caused by less dispersion in the ring was to be expected due to the finite resolving power of the diffraction gratings used in the grating compressor. However, the results of this basic experimental setup demonstrate the feasibility of generating an unequally spaced frequency comb with an intra-cavity grating compressor.

4.2.2 Algebraic simulation

One major difference between interference of two frequency combs as described in Chapter 3 and interference of only one unequally spaced frequency comb is that the beating signals for the latter case are in general narrower spaced. The experimental results of the two CW frequency comb beating presented in 3.3.2 showed a spacing of the beating signals $\delta = 5 – 10$ MHz. When CW c-FTS is conducted with beating of one unequally spaced frequency comb, spacing of the beating signals is determined by the change in FSR from one beating pair to the next one. This change in FSR is a function of the dispersion in the cavity. From first principle experiments of the intra-cavity grating compressor, it could be estimated that the beating signals in the first order replica are spaced at about 1 kHz. Experimental results of a ring cavity with a dispersive fiber spool instead of the grating compressor showed that the beating signals were spaced at about 0.01 Hz. Taking also the frequency resolution of the FFT into account, a narrower spacing causes a reverse relation between frequency resolution and spectral signal density. In the two combs setup, every frequency downshifted band was theoretically resolvable in the FFT. However, in the one comb setup, quite a few bands are accumulated by one frequency discretization point in the FFT. The exact number of signals per frequency resolution (SPFR) depends on the experimental setup and on the sample frequency and measurement time.

To evaluate the effect of spectral signal density in combination with frequency resolution of the FFT and phase distribution of the signals on the performance of CW c-FTS, the interference of an unequally spaced CW frequency comb was simulated according to equation (2.6). The optical frequency comb consisted of 50 modes, which were unequally

spaced. All amplitudes were set to 1 and three different phase distributions were simulated: all phases equal to zero, all phases random [0 0.2π], and all phases random [0 2π]. A Blackman window was applied to the time trace of the output intensity to minimize spectral leakage. Blackman windows have slightly wider central lobes and less sideband leakage than equivalent length Hamming and Hann windows. The frequency resolution in the FFT was 0.1 Hz. The results of this simulation are presented in Figure 4.4 where different replica orders are displayed. The higher the replica order, the larger the footprint in the Fourier domain and hence, the smaller the spectral signal density (see Figure 4.1). In Figure 4.4a) the third order replica is shown that is formed by 50-3 = 47 beating signals. The footprint of this order is ~3 Hz, therefore 31 discretization points in the FFT. The SPFR in this case is $\frac{47}{31} = 1.5$ (see top right corner of Figure 4.4a)). A comparison of Figure 4.4a)-d) shows that the bigger the SPFR, the higher the affect of the phase distribution of the ***E*** field components on the replica of the original comb in the optical frequency range. For a small SPFR (see Figure 4.4d) and simulation results in 3.2) replicas with different phase distributions converge. For SPFR > 1.5 the mode-locked case only shows spectral content at the beginning and the end of the replica, whereas for a random phase distribution [0 2π] there is spectral content over the whole footprint range but the power is distributed rather randomly.

These simulation results are important for the interpretation of experimental data when the spectral signal density is high in relation to the frequency resolution of the FFT. Because of the random phase distribution [0 2π] that has to be assumed for the modes of an unequally spaced CW frequency comb, the replicas should be expected to look “noisy”.

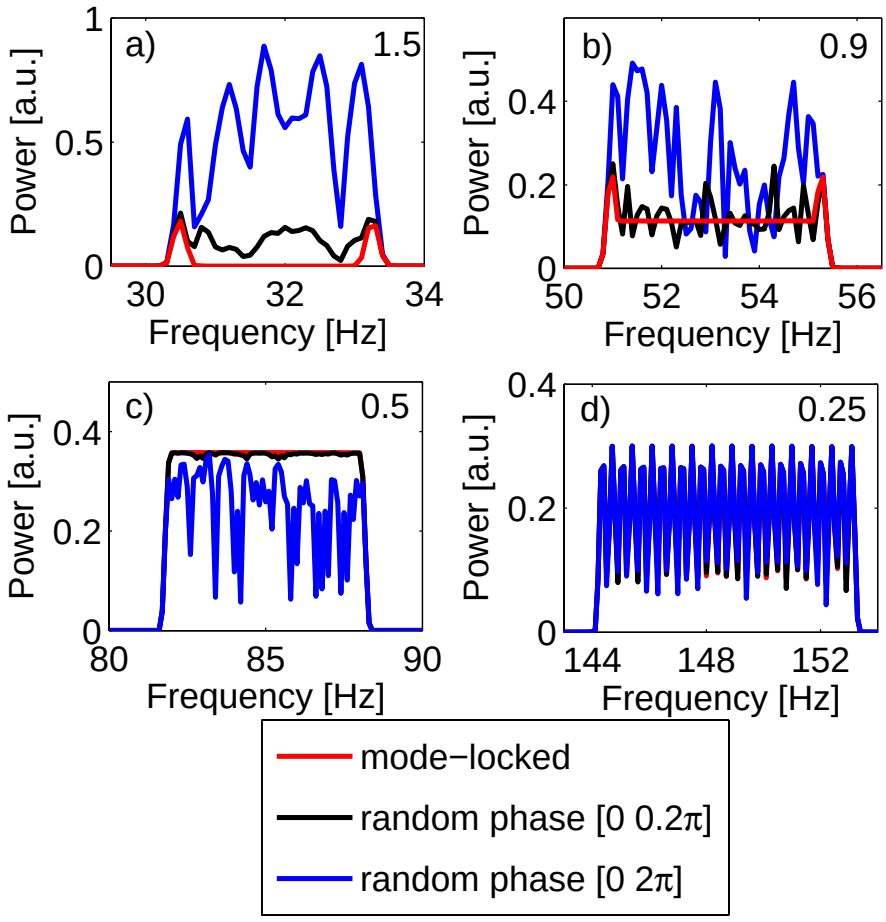

Figure 4.4 Algebraic simulation results for different phase settings for the *E* field components in the ring cavity. A Blackman window was applied to the time trace of the output intensity to minimize spectral leakage. Although all amplitudes were set equal to 1, a comparison of (a)-(d) shows that the FFT results strongly depend on the relation between spectral signal density and frequency resolution, indicated in the upper right corner of the plots.

However, absorption can still be obtained without major implications if the transmittance and reference are measured at the same time. Averaging of FFTs obtained from different time traces as well as averaging of different replica orders can smooth the shape of the replica if a spectrum has to be obtained.

4.3 EXPERIMENT

This section presents the setup and the results of a hyperspectral light source where a highly dispersive ring cavity generates an unequally spaced frequency comb. Beating of this frequency comb frequency-downshifts the native spectrum in the optical frequency range and by so doing allows CW c-FTS.

4.3.1 Setup

The design, which is shown in Figure 4.5a), relies on a ring cavity that is formed by a semiconductor-based linear optical amplifier (LOA, Finisar/Genoa G111[37]), a polarization controller (PC, Fiber Control FPC) for maintaining a linear polarization in the mode cavity, a grating compressor (GC), and an isolator (ISO, AOC Tap-WDM-Isolator Hybrid) that guarantees unidirectional lasing operation. Due to the grating dispersion, the length of the cavity is wavelength-dependent, since different colors have different path lengths through the GC as can be seen in Figure 4.5b). The (equivalent free space) length of the cavity varied from 5.10 m at 1530 nm to 5.28 m at 1570 nm.

The efficiency of the gratings used in the grating compressor (1200 g/mm; blaze wavelength: 750 nm) is strongly polarization dependent. The layout of the grating compressor was designed for an operating wavelength range from 1530–1570 nm. In this spectral range, the reflectance efficiency for the *S* and *P* polarization plane is ~95% and ~5% respectively. Therefore, the grating compressor that employed four diffraction gratings as shown in Figure 4.5b) acted as a polarizer with an extinction of ~ 1.3 x 10^5:1. The polarization controller in the ring cavity was tuned to compensate for the rotation of the polarization axis in the fiber coupled part of the cavity.

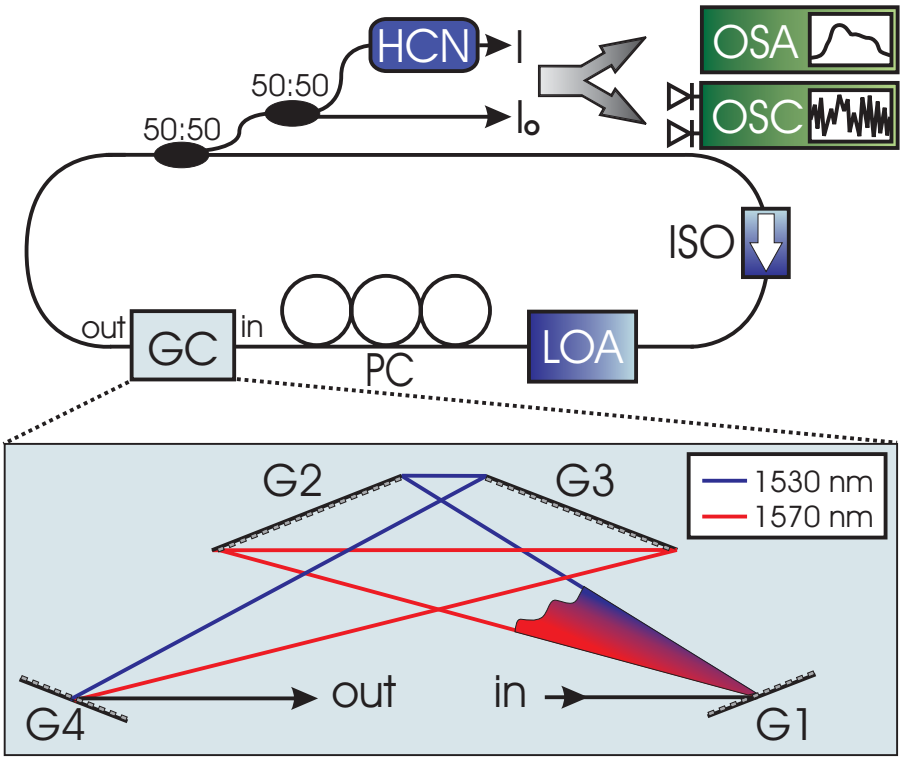

Figure 4.5 Experimental setup. (a) Sketch of the ring cavity that generates an unequally spaced frequency comb. The beating of this comb is then used to measure the absorption spectrum of hydrogen cyanide HCN_{13} via a fast Fourier transformation of the time domain signals: reference I_o and transmitted I recorded with two photo-receivers and an oscilloscope (OSC). Absorption is also spectrally analyzed with an optical spectrum analyzer (OSA). (b) Layout of the grating compressor following[8].

To show the feasibility of CW c-FTS, transmitted I and reference I_o of hydrogen cyanide HCN_{13} were monitored with a data acquisition system, consisting of two photo-receivers (New Focus 1592; 3.5 GHz bandwidth and New Focus 1544; 12 GHz bandwidth) and a real-time sampling oscilloscope (Tektronix TDS7404; 4 GHz bandwidth, 10 GSample / s on each of 2 channels). The time traces captured with this device were then Fourier transformed. I and I_o are also recorded with an optical spectrum analyzer (OSA; Agilent 86142B, ~ 8 GHz spectral resolution).

A picture of the experimental setup of the ring cavity with the grating compressor is shown in Figure 4.6. It can be seen that a couple of *XY* and *XYZ* stages were used for the alignment of the setup. In particular, the alignment of the grating compressor turned out to be rather difficult.

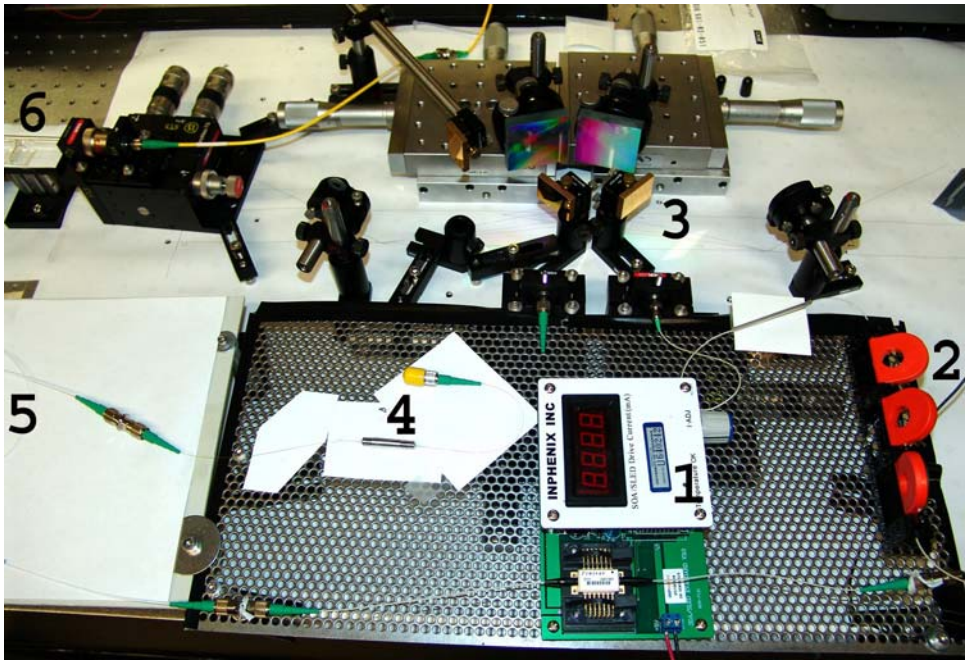

Figure 4.6 Picture of experimental setup. (1) Linear optical amplifier and driver board; (2) Polarization controller; (3) Grating compressor; (4) Optical isolator; (5) 50:50 output splitter; (6) HCN_{13} gas cell

The HCN_{13} gas cell setup is shown in Figure 4.7. Light from the input fiber (white insulation), which contained half the output of the ring cavity, was collimated and directed through the gas cell. The transmitted signal *I* was then coupled into the output fiber (yellow insulation) and recorded with the data acquisition systems. All fibers used in the setup were single mode.

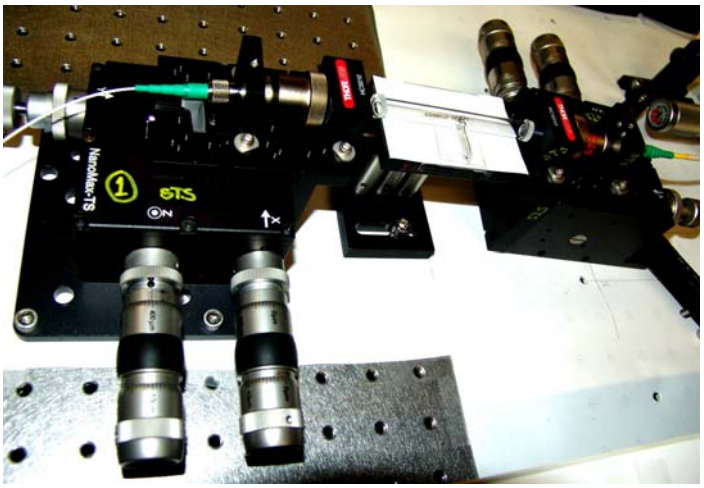

Figure 4.7 Picture of HCN_{13} gas cell setup.

4.3.2 Results

The first 100 ns section of the 1 ms time trace of the transmitted I and reference I_o signals captured with the OSC are shown in Figure 4.8. In the time domain, these two signals do not seem to carry any information.

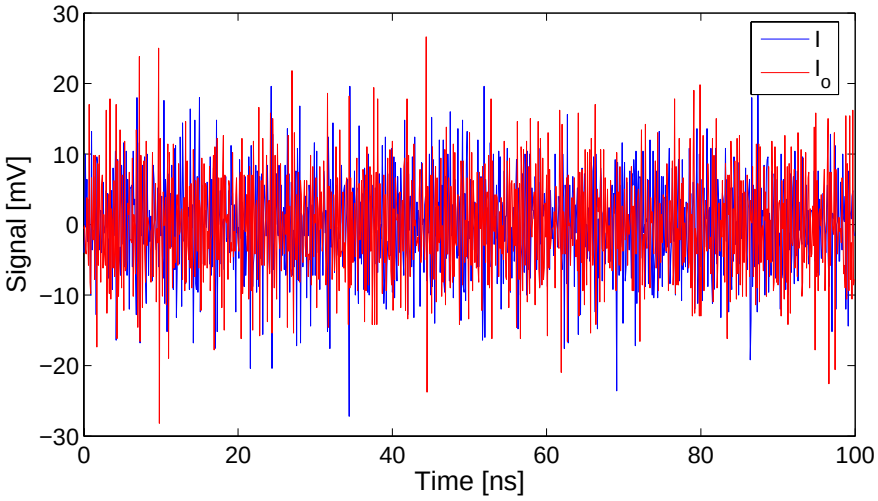

Figure 4.8 Transmitted signal I and reference signal I_o in the time domain.

The spectral results of this experiment are shown in Figure 4.9. Lasing operation was achieved over about 0.4 THz as it can be seen in transmitted I and reference I_o spectra monitored with the OSA (750 ms) in Figure 4.9a).

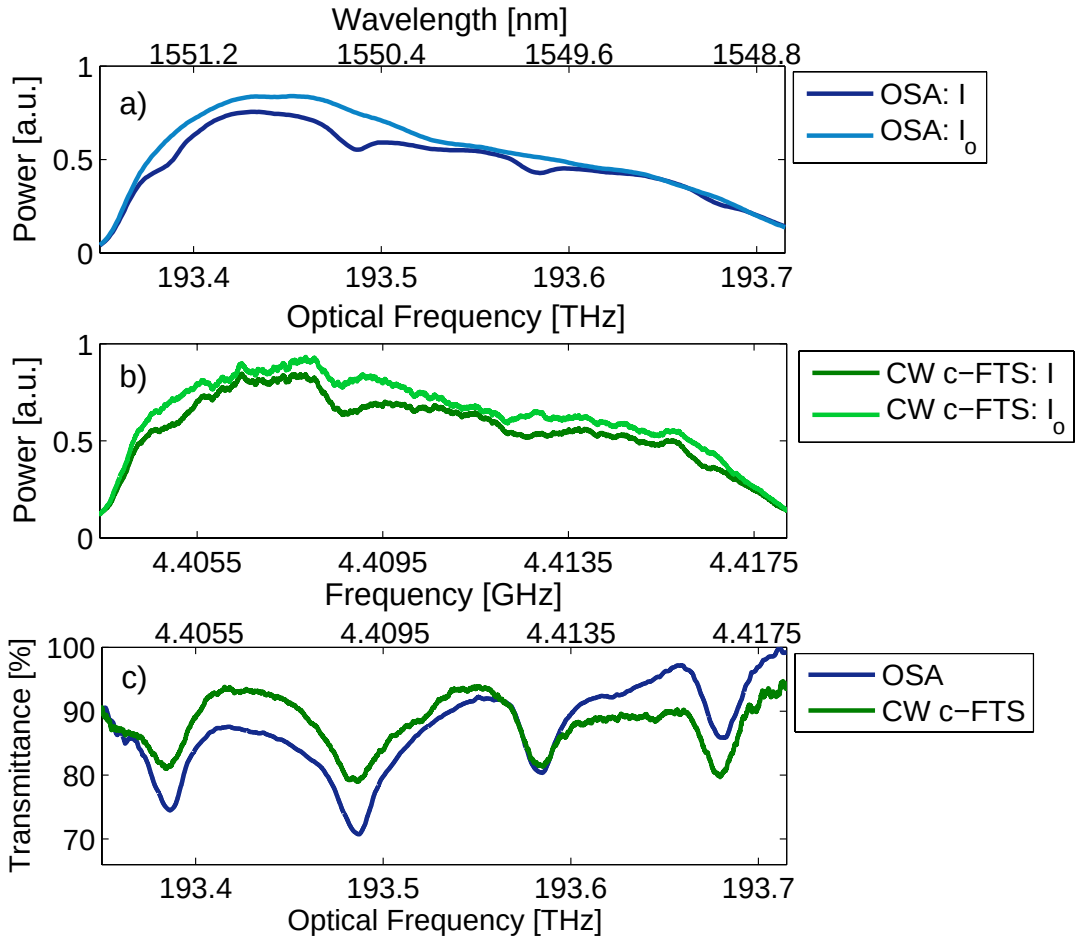

Figure 4.9Transmitted I, reference I_o, and transmittance spectra of hydrogen cyanide. (a) I and I_o recorded with an optical spectrum analyzer in 750 ms. (b) I and I_o of 97th order via Fourier transformations of CW c–FTS signals measured with photo-detectors in 1 ms. (c) Comparison of OSA and CW c–FTS transmittance spectra I / I_o

The LOA gain was > 10 dB, the insertion loss of the grating compressor -7 dB and the total output power of the cavity ~ 3 mW. The Fourier transformation of the CW c-FTS time

signals (1ms) showed a first order replica of the optical frequency comb at 57.5–58.1 MHz which results in an average FSR of the optical frequency comb of 57.8 MHz. This number in combination with the 0.4 THz spectral coverage gives an estimate of ~ 6920 total fringes composing the optical frequency comb. The beating of each fringe of the optical frequency comb with itself was observed at DC–500 kHz with a FWHM of 380 kHz. This gives a measure for the linewidth of individual cavity modes. From this observation, we estimated the effective finesse of the ring cavity to be 152 under lasing conditions. The replica of the native I and I_o presented in Figure 4.9b) is the 97^{th} order at 5.582–5.597 GHz but is aliased back to 4.403–4.418 GHz because of the 5 GHz Nyquist frequency of the oscilloscope. The replica was mirrored to compensate for the folding about the Nyquist frequency and a moving average filter was applied to smooth out the comb structure. Simulations showed that for the presented 97^{th} order, the mode spacing at both extremes of the replica is 2.325 kHz at 5.582 GHz and 2.327 kHz at 5.597 GHz, thus the spectral distribution is uniform in frequency.This higher order replica has a larger footprint (15 MHz) in the Fourier domain than the first order replica and the effective finesse is improved by a factor of the order number, 97. Compared to the SNR of the time domain signals of I and I_o (18.75 dB), the SNR of this order was improved by a factor of 4.2 to 25 dB because the inherent noise in the data acquisition system was lower at high frequencies. The SNR was obtained by comparing the average signal power of the 97^{th} order to the noise floor in the FFT. The comparison of OSA and CW c-FTS transmittance spectra (I / I_o) in Figure 4.9 (c) shows absorption dips in both spectra that have about the same width.

4.4 CONCLUSION

In conclusion, the feasibility of CW c-FTS was demonstrated by measuring absorbance of hydrogen cyanide. Compared to the spectrum recorded with an OSA, the CW c-FTS measurement speed was significantly faster (OSA: 750 ms; CW c-FTS: 1 ms) with a similar spectral resolution. Transmittance spectra were recorded spectra based on CW c-FTS in 10 μs but the quality was poor, probably due to mode competition in the LOA and due to lower frequency resolution in the FFT. In ongoing work, we plan to improve the stability and spectral coverage of the comb to yield high-quality, broadband spectra in shorter measurement times.

CHAPTER 5. CONCLUSIONS AND FUTURE WORK

Continuous-wave comb Fourier transform spectroscopy (CW c-FTS) encodes spectral information in frequency that allows a simultaneous measurement of all spectral bands in the wavelength range of operation. Like conventional FTS, this new approach offers broad spectral coverage and high throughput. However, CW c-FTS also provides high repetition rates, an enhanced finesse when using replicas of higher orders, and a good signal-to-noise ratio (SNR). SNR is improved compared to conventional spectrometers due to the high spectral radiance of the light sources employed in CW c-FTS sensor systems. Also, it yields an always readily available signal because the comb structure in the laser ring does not change once it is built-up from the amplified spontaneous emission of the intra-cavity amplifier. CW c-FTS also offers fewer drawbacks when compared to recently developed frequency-swept hyperspectral lasers[32, 39-43], which show in general one or more of the following disadvantages: Moving parts; one scan direction superior to other; unreliable at rapid sweep speeds; constrained sweep rates; wavelength sweeps generally too fast; undesirable polarization effects; unsuitable outside of telcom bands; unstable spectral resolution. In principle, CW c–FTS techniques can circumnavigate all of these drawbacks.

With a better understanding of CW frequency combs, which provides the basis of engineering stable broadband combs, this technique holds the possibility of a universal and simple approach for spectroscopy at almost arbitrary measurement speeds and spectral resolutions limited only by Fourier principles.

This work introduced CW c-FTS and concentrated on the initial development of this new spectroscopy approach. The results of computer modeling and basic experimental setups

were used to derive basic properties of the interference of CW frequency combs, but also to design first hyperspectral light sources based on CW c-FTS. The implementation of two different designs demonstrated, in addition to the feasibility of CW c-FTS, the competitiveness of this approach to an optical spectrum analyzer, representing a conventional spectroscopic technique.

CW c-FTS is still in its infancy. Although the results presented in this thesis already look very promising, the research on the CW c-FTS idea is far from complete. Three main topics of future work should be:

- **Better understanding of CW frequency combs:** More simulations have to be conducted to forecast performance limits of CW c-FTS. In particular the effects of stability and finesse of the comb structure on the performance of CW c-FTS have to be investigated.

- **Improved comb stability:** More stable combs will ultimately lead to higher repetition rates and a better SNR. An entirely free space based ring laser eliminates all polarization issues and thus should increase comb stability. Also, a version based on fiber Raman amplification rather than LOA gain medium should offer improved comb stability.

- **Broader spectral coverage:** To create the opportunity to detect multiple species, broad spectral features the spectral coverage of the CW frequency comb has to be enhanced.

First steps in the direction of a broader spectral coverage have already been made by using closed-loop control of an intra-cavity programmable spectral filter[44]. The idea of this approach is that by attenuating only the lasing part of the spectrum regions nearby become more attractive for the gain medium to amplify, which results in an enhancement of the spectral coverage of the frequency comb.

The setup is depicted in Figure 5.1. An optical spectral profiler (OSP; spectral resolution: 0.1 nm; spectral coverage: 1520–1620 nm; maximum attenuation: -30 dB with a 0.1 dB resolution) was included in the ring cavity formed by a linear optical amplifier (LOA), a polarization controller (PC), and isolator (ISO) and an output coupler.

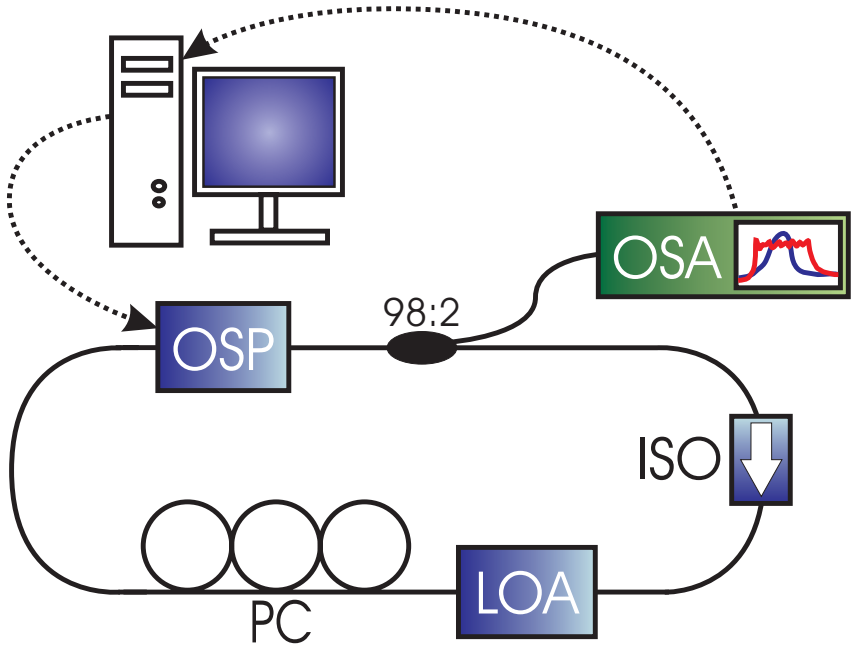

Figure 5.1 Experimental setup for broadening the spectral coverage of a CW frequency comb. Closed loop control can be implemented with an intra-cavity optical spectral profiler (OSP).

The control loop was closed with an optical spectrum analyzer (OSA) and a computer to execute the control law and to communicate with the OSP. Because there was no

mathematical model of the physical system, the control law was constructed intuitively. Due to the high sensitivity of the system, a pure integral controller was implemented, where the corresponding gain was adapted over time to prevent overshoot.

The results are presented in Figure 5.2. The blue line in Figure 5.2 shows the lasing spectrum of the ring laser with zero filter attenuation. After 127 loop iterations, the FWHM of the lasing spectrum was broadened from originally 18 nm to 61 nm.

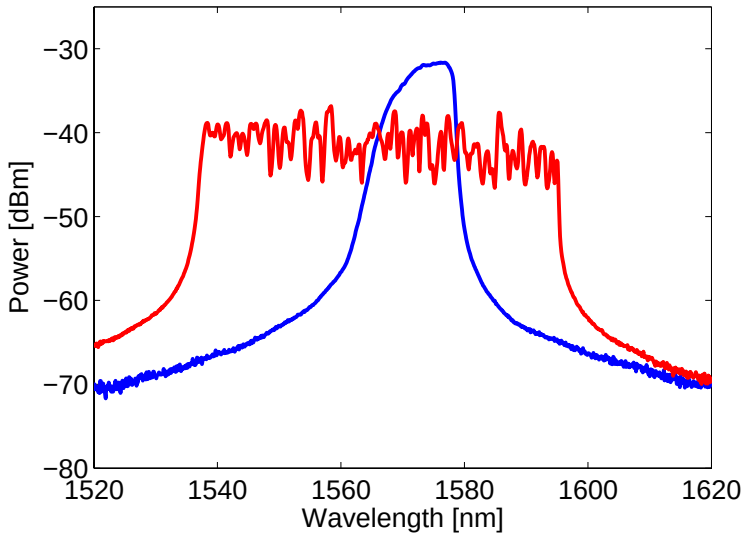

Figure 5.2 Broadening of CW frequency comb from 18 nm (blue line, zero filter attenuation) to 68 nm (red line) after 127 loop iterations.

REFERENCES

1. G. W. Chantry, "Long-wave optics: the science and technology of infrared and near-millimetre waves", **1**, 790 (1984).

2. A. A. Christy, Y. Ozaki, and V. G. Gregoriou, *Modern Fourier Transform Infrared Spectroscopy,* (Elsevier Science, 2001).

3. P. R. Griffiths, B. L. Hirsche, and C. J. Manning, "Ultra-rapid-scanning Fourier transform infrared spectrometry", Vibrational Spectroscopy, **19:1**, 165-176 (1999).

4. T. N. Buican and A. H. Carrieri, "Ultra-High Speed Solid-State FTIR Spectroscopy and Applications for Chemical Defense", Anonymous (2004), pp. 9.

5. A. Schliesser, M. Brehm, F. Keilmann, and van der Weide, D. W., "Frequency-comb infrared spectrometer for rapid, remote chemical sensing", Opt Expr, **13:22**, 9029-9038 (2005).

6. van der Weide,Daniel W., J. Murakowski, and F. Keilmann, "Gas-absorption spectroscopy with electronic terahertz techniques", IEEE Trans Microwave Theory Tech, **48:4 pt 2**, 740-743 (2000).

7. van der Weide, D. W. and F. Keilmann, "Coherent Periodically Pulsed Radiation Spectrometer", **545136:US patent no. 5784309** (1998).

8. E. B. Treacy, "Optical Pulse Compression with Diffraction Gratings", IEEE J.Quantum Electron, **QE-5**, 454-458 (1969).

9. van der Meer, F. and S. de Jong, *Imaging Spectrometry: Basic Principles and Prospective Applications,* (Kluwer Academic Publishers, Dordrecht, 2004).

10. A. D. Meigs, L. J. Otten III, and T. Y. Cherezova, "Ultraspectral imaging: a new contribution to global virtual presence", Aerospace Conference, Proceedings, IEEE, **2**, 5-12 (1998).

11. G. Vane and A. F. H. Goetz, "Terrestrial Imaging Spectrsocopy", Rem Sens Environ, **24**, 1-29 (1988).

12. G. R. Taylor and D. Vukovic, "Mine site mapping with hyperspectral imagery", IGARSS '01 IEEE 2001 International, **2**, 634-636 (2001).

13. K. H. Scholte, A. Hommels, Van der Meer, F.D., E. C. Slob, S. B. Kroonenberg, E. Aliyeva, D. Huseynov, and I. Guliev, "Subsurface resistivity in combination with hyperspectral field and satellite data for mud volcano dynamics, Azerbaijan", GARSS '03 Proceedings 2003 IEEE International, **5**, 3395- 3397 (2003).

14. K. Makisara and E. Tomppo, "Airborne Imaging Spectrometry in National Forest Inventory", IGARSS, **2**, 1010-1013 (1996).

15. C. N. Banwell and E. M. McCash, *Fundamentals of molecular spectroscopy* (McGraw-Hill, London; New York, (1994).

16. P. P. Ward, "Plasma process control with optical emission spectroscopy", Seventeenth IEEE/CPMT International, 166-169 (1995).

17. A. H. Westphal, A. Matorin, M. A. Hink, J. W. JBorst, van Berkel, W. J. H., and Visser, A. J. W. G., "Real-time Enzyme Dynamics Illustrated with Fluorescence Spectroscopy of *p*-Hydroxybenzoate Hydroxylase", J Biol Chem, **281:16**, 11074-11081 (2006).

18. T. Encrenaz, B. Bezard, T. Owen, S. Lebonnois, F. Lefevre, T. Greathouse, M. Richter, J. Lacy, S. Atreya, A. S. Wong, and F. Forget, "Infrared imaging spectroscopy of Mars: H2O mapping and determination of CO2 isotopic ratios", Icarus, **179:1**, 43-54 (2005/12/1).

19. R. Huber, M. Wojtkowski, and J. G. Fujimoto, "Fourier Domain Mode Locking (FDML): A new laser operating regime and application for optical coherence tomography", Opt Express, **14:8**, 3225-3237 (2006).

20. D. M. Livingston, *The Master of Light: A Biography of Albert A. Michelson,* (Scribner, New York, 1973).

21. M. Heideman, D. Johnson, and C. S. Burrus, "Gauss and the history of the FFT", IEEE Signal Processing Magazine, **1**, 14-21 (1984).

22. J. W. Cooley and O. W. Tukey, "An Algorithm for the Machine Calculation of Complex Fourier Series", Math Comput, **19**, 297-301 (1965).

23. C. Smith, *Fundamentals of Fourier Transform Infrared Spectroscopy,* (CRC, Boca Raton, 1996).

24. P. B. Fellgett, *The multiplex advantage,* in Ph.D., (University of Cambridge, Cambridge, 1951).

25. P. Jacquinot, "The etendue advantage" *in XVII Meeting of Congrès du Groupment avancement des méthodes d'analyse spectrométriques,* Anonymous Paris (1954).

26. L. N. Mertz, G. H. Nakano, and J. R. Kilner, "Rotational aperture synthesis for x rays", J Opt Soc Am A, **3:12**, 2167-2170 (1986).

27. M. J. Murphy, D. Datlowe, J. Hamilton, and S. Roselle, "A modular rotating collimator imaging x-ray spectrometer", SPIE proceedings, San Diego, Ca, **1743:53**, 501 (1992).

28. G. J. Hurford, E. J. Schmahl, R. A. Schwartz, A. J. Conway, M. J. Aschwanden, A. Csillaghy, B. R. Dennis, C. Johns-Krull, S. Krucker, R. P. Lin, J. McTiernan, T. R. Metcalf, J. Sato, and D. M. Smith, "The RHESSI Imaging Concept", Solar Physics, **210:1**, 61-86 (2002).

29. A. T. Forrester, R. A. Gudmundsen, and P. O. Johnson, "Photoelectric Mixing of Incoherent Light", Phys Rev, **99:6**, 1691-1700 (1955).

30. L. A. Kranendonk, R. J. Bartula, and S. T. Sanders, "Modeless operation of a wavelength- agile laser by high-speed cavity length changes", Opt Express, **13:5**, 1498-1507 (2005).

31. J. P. Smith and V. Hinson-Smith, "The endearing FTIR spectrophotometer", Anal Chem, **75:1**, 37-39 (2003).

32. L. A. Kranendonk, A. W. Caswell, A. N. Myers, and S. T. Sanders, "Wavelength-agile laser sensors for measuring gas properties in engines", SAE 2003 Transactions Journal of Engines, 1578-1583 (2003).

33. E. Hecht, *Optics* (Addison-Wesley, Reading, Mass., 2002).

34. S. T. Sanders and J. W. Walewski, "Method and apparatus for conducting heterodyne frequency-comb spectroscopy", **US patent, submitted** (2006).

35. K. K. Qureshi, H. Y. Tam, W. H. Chung, and P. K. A. Wai, "Multiwavelength laser source using linear optical amplifier", IEEE Photonics Technology Letters, **17:8**, 1611-1613 (2005).

36. Th. Kraetschmer, J. W. Walewski, and S. T. Sanders, "All-fiber laser for generating interlaced continuous-wave frequency combs and application to Fourier-transform spectroscopy", Optical Engineering, **45:5**, 050502 (2006).

37. A. K. Verma, R. P. Ratowsky, D. A. Francis, S. P. Dijaili, and J. D. Walker, "Developments in linear optical amplifier technology" *in Semiconductor Optoelectronic Devices for Lightwave Communication, Sep 8-10 2003,* Anonymous (The International Society for Optical Engineering, 2003), pp. 203-217.

38. Th. Kraetschmer, J. W. Walewski, and S. T. Sanders, "Continuous-Wave Frequency Comb Fourier Transform Source based on a High-Dispersion Cavity", Optics Letters, **accepted** (2006).

39. S. T. Sanders, "Wavelength-Agile Fiber Laser using Group-Velocity Dispersion of Pulsed Super-Continua and Application to Broadband Absorption Spectroscopy", Appl.Phys.B**, 75**, pp. 799-802 (2002).

40. J. W. Walewski and S. T. Sanders, "High-Resolution Wavelength-Agile Laser Source Based on Pulsed Super-Continua", Appl.Phys.B**, 79:4,** pp. 415-418 (2004).

41. M. Asano and S. Yamashita, "Wide and Fast Wavelength-Tunable Mode-Locked Fiber Laser using Dispersion Tuning"*, Fiber Lasers III: Technology, Systems, and Applications, Jan 23-26 2006*, Anonymous eds., San Jose, CA, United States**, 6102**, 610218 (2006).

42. R. Huber, M. Wojtkowski, and J. G. Fujimoto, "Fourier Domain Mode Locking (FDML): A New Laser Operating Regime and Application for Optical Coherence Tomography," Opt. Express**, 14:8**, pp. 3225-3237 (2006).

43. L. A. Kranendonk, R. Huber, J. G. Fujimoto, and S. T. Sanders, "Wavelength-Agile H_2O Absorption Spectrometer for Thermometry of General Combustion Gases", Proc. Comb. Inst.**, 31** (2006).

44. Th. Kraetschmer, and S. T. Sanders, "Enhancing the Spectral Coverage of a CW Frequency Comb using Closed-Loop Control of an intracavity programmable spectral Filter," IEEE Photonics Technology Letters**, in preparation**.